AD-A131 466 SPECTROSCOPIC STUDIES OF LASING TRANSITIONS IN THE DIATOMIC MERCURY HALIDES(U) VANDERBILT UNIV NASHVILLE TN DEPT OF CHEMISTRY J TELLINGHUISEN AUG 83 1/1

UNCLASSIFIED N00014-81-K-0477 F/G 7/4 NL

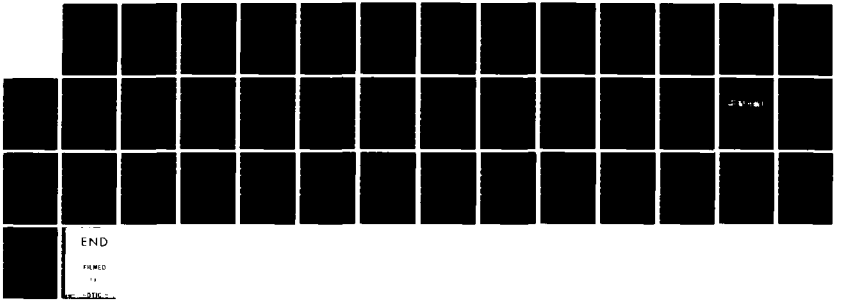

END

FILMED

DTIC

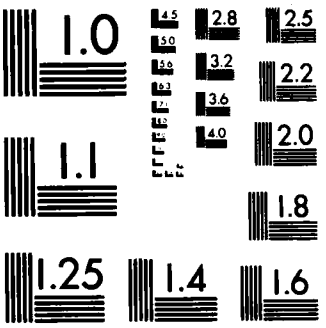

MICROCOPY RESOLUTION TEST CHART
NATIONAL BUREAU OF STANDARDS-1963-A

(12)

Report N00014-81-K-0477-2

SPECTROSCOPIC STUDIES OF LASING TRANSITIONS IN THE DIATOMIC MERCURY HALIDES

Joel Tellinghuisen
Department of Chemistry
Vanderbilt University
Nashville, Tennessee 37235

August, 1983

Annual Summary Report for Period May 1, 1982 to April 30, 1983

Approved for public release; distribution unlimited

Prepared for:

Office of Naval Research
Physics Program Office (Code 421)
800 North Quincy Street
Arlington, Virginia 22217

SECURITY CLASSIFICATION OF THIS PAGE *(When Data Entered)*

REPORT DOCUMENTATION PAGE		READ INSTRUCTIONS BEFORE COMPLETING FORM
1. REPORT NUMBER N00014-81-K-0477-2	2. GOVT ACCESSION NO. AD-A131466	3. RECIPIENT'S CATALOG NUMBER
4. TITLE *(and Subtitle)* SPECTROSCOPIC STUDIES OF LASING TRANSITIONS IN THE DIATOMIC MERCURY HALIDES		5. TYPE OF REPORT & PERIOD COVERED Annual Summary -- May 1, 1982 - April 30, 1983. 6. PERFORMING ORG. REPORT NUMBER
7. AUTHOR(s) Joel Tellinghuisen		8. CONTRACT OR GRANT NUMBER(s) N00014-81-K-0477
9. PERFORMING ORGANIZATION NAME AND ADDRESS Department of Chemistry Vanderbilt University Nashville, Tennessee 37235		10. PROGRAM ELEMENT, PROJECT, TASK AREA & WORK UNIT NUMBERS ? ? ? ? ? ? ? ? ? ? ? ? ? ? ? ?
11. CONTROLLING OFFICE NAME AND ADDRESS Office of Naval Research, Physics Program Office, Arlington, Virginia 22217		12. REPORT DATE August, 1983 13. NUMBER OF PAGES 40
14. MONITORING AGENCY NAME & ADDRESS(*if different from Controlling Office*)		15. SECURITY CLASS. (*of this report*) 15a. DECLASSIFICATION/DOWNGRADING SCHEDULE

16. DISTRIBUTION STATEMENT *(of this Report)*

Approved for public release; distribution unlimited

17. DISTRIBUTION STATEMENT *(of the abstract entered in Block 20, if different from Report)*

18. SUPPLEMENTARY NOTES

19. KEY WORDS *(Continue on reverse side if necessary and identify by block number)*

mercury halides, HgCl, HgBr, HgI, electronic transition lasers, electronic spectroscopy, diatomic spectroscopy, vibrational analysis, rotational analysis, emission spectroscopy, Franck-Condon factors

20. ABSTRACT *(Continue on reverse side if necessary and identify by block number)*

The B $^2\Sigma^+$ X $^2\Sigma^+$, C $^2\Pi_{3/2}$ X $^2\Sigma^+$, and D $^2\Pi_{1/2}$ X $^2\Sigma^+$ emission transitions of HgCl, HgBr, and HgI have been photographed and analyzed for single isotopomers containing ^{200}Hg. New methods have been devised for fitting data and approximating potential curves for heavy diatomics like the HgX molecules. Results for these molecules offer significant improvements in the spectroscopic parameters and related properties, such as Franck-Condon factors and dissociation energies.

DD FORM 1 JAN 73 1473 EDITION OF 1 NOV 65 IS OBSOLETE

S/N 0102-LF-014-6601

SECURITY CLASSIFICATION OF THIS PAGE *(When Data Entered)*

Progress Summary

In the first year of this project (May, 1981 - April, 1982), our efforts were concentrated on the reanalysis of the B→X transitions of HgCl, HgBr, and HgI, working with single isotopomers containing ^{200}Hg. These transitions were vibrationally reanalyzed in all three molecules, leading to significant changes in the spectroscopic parameters, particularly for the ground ($X\ ^2\Sigma^+$) states. At the same time work was begun on the rotational analyses of HgCl and HgBr. While these results gave an improved description of the B($^2\Sigma^+$) and X states, they were not really adequate for the latter. The reason was that the B→X transitions do not sample the low-v (<7) regions of the X states, because these levels are out of the Franck-Condon region for emission from the low v' levels that are mainly populated in our Tesla discharge sources (and in HgX lasers).

To obtain spectroscopic constants for low levels of the X states, we originally considered transient B←X absorption experiments. However these experiments would have required equipment that we did not have and were unable to fabricate in the time available. Consequently we turned our attention to the C($^2\Pi_{1/2}$)→X and D($^2\Pi_{3/2}$)→X transitions, which occur in the UV for all three HgX molecules, and which were present in the emission from our sources with sufficient intensity to permit photographing them at high resolution. In every case these transitions show violet-degraded band structure and terminate on low v levels of the X state. Therefore, by combining results for these systems with those for B→X, we have been able to obtain improved constants, valid typically for v = 0-35 of the X state. We have prepared a preliminary report of this work on HgBr, which also describes a new method we have used for fitting the data. This paper is included as an appendix to the present report. We have more or less completed work on the D→X systems in HgCl and HgBr, and the C→X and several weaker systems in HgI; and we expect to prepare papers for publication soon. The C→X systems in HgCl and HgBr, and D→X in HgI are still under investigation. Work continues also on the rotational analyses for HgCl and HgBr.

I mentioned the development of a new method for representing vibrational energy levels in molecules like HgBr(X), where the data sample a large fraction of the total binding energy of the state. This method is the use of a mixed representation for the levels -- the customary polynomials in (v+1/2) for low levels, near-dissociation expansions [which involve polynomials in (v_D-v), where v_D is the noninteger vibrational quantum number at the dissociation limit] for high v. In conjunction with the development of this method, I earlier devised computational schemes for direct fitting of spectroscopic data to near-dissociation expansions, with application to the D'→A' transitions in

I_2 and Br_2 and the B→X and D→X systems in XeCl. This work has now been published and is included as an appendix to this report.

Another new method we have developed is the use of Morse-RKR potential curves. We have found that the repulsive (left) branches of many known diatomic potential curves can be very well approximated by a Morse curve derived from the known R_e, ω_e, and $\omega_e x_e$ values. For heavy diatomics such as the HgX molecules it may be relatively easy to obtain vibrational constants but hard to obtain rotational constants, because the spectra are so congested. In such cases one can with fair reliability approximate the repulsive branch of the potential by a Morse curve (guessing the unknown R_e), then obtain the attractive branch from the RKR f integrals (which are calculated from the vibrational constants alone). A paper describing this method has been published and is included as an appendix to this report.

Future Work

Work continues on the rotational analyses of B→X in HgBr and HgCl. We have succeeded in computerizing our line-measuring procedures and are preparing to apply our new instrumentation to the line-rich HgCl spectrum, and possibly to HgBr (where, however, line congestion makes necessary more operator intervention). We have also now (finally) set up and begun testing our Fabry-Perot interferometer. We hope to begin using it to resolve blended lines and to measure line widths as a function of pressure within a few weeks. We have also recorded HgBr and HgI emission spectra at low resolution as a function of pressure. We will use these and additional data to extract extimates of the R-dependence of the B→X transition strength function.

Personnel

Three graduate students -- K. S. Viswanathan, J. Gail Ashmore, and O. Carlysle Salter -- have been employed essentially full time on this project. Dr. Viswanathan has now completed the requirements for his Ph. D. degree (thesis: "Part 1: Spectroscopic Studies of Charge Transfer Transitions in Iodine, Bromine, and Mercury Iodide; Part 2: Nitrogen Laser Pumped Dye Laser," June, 1983), and has taken a postdoctoral appointment in the Department of Chemistry at the University of Indiana. Ashmore and Salter will soon begin their fourth years, but Salter will be supported under another project. My wife, Patricia C. Tellinghuisen, was employed one-fourth time until March,

1983, at which time she began to be supported under another project (but funded as an extension of this project; see below).

Other Support

I have received funding from DARPA for a project called "XeF Spectroscopy," which is funded as an extension to the present project for the period March 1, 1983 - November 30, 1983. I have also obtained funding from the Air Force Office of Scientic Research for "Spectroscopic Studies of the Halogens," for the period April 1, 1983 - March 31, 1986.

Publications - Cummulative Listing

1. "The B→X transition in $^{200}Hg^{79}Br$," by Joel Tellinghuisen and J. Gail Ashmore, Appl. Phys. Lett. 40, 867 (1982).
2. "B→X transitions in HgCl and HgI," by Joel Tellinghuisen, Patricia C. Tellinghuisen, Sue A. Davies, Patrick Berwanger, and K. S. Viswanathan, Appl. Phys. Lett. 41, 789 (1982). (Appendix 1)
3. "The Use of Morse-RKR Curves in Diatomic Calculations," by Joel Tellinghuisen and Stuart D. Henderson, Chem. Phys. Lett. 91, 447 (1982). (Appendix 2)
4. "Spectroscopic Studies of Lasing Transitions in the Diatomic Mercury Halides," by Joel Tellinghuisen (Annual summary report for period May 1, 1981 to April 30, 1982), Report N00014-81-K-0477-1, AD No. AD A116297.
5. "Direct Fitting of Spectroscopic Data to Near-Dissociation Expansions: $I_2(D'\rightarrow A')$, $Br_2(D'\rightarrow A')$, and XeCl (B→X and D→X)," by Joel Tellinghuisen, J. Chem. Phys. 78, 2374 (1983). (Appendix 3)
6. "The $B(^2\Sigma^+) \rightarrow X(^2\Sigma^+)$ Transition (4050-4500 Å) in HgI," by K. S. Viswanathan and Joel Tellinghuisen, J. Mol. Spectrosc. 98, 185 (1983). (Appendix 4)
7. "Mercury Halide Spectroscopy," by Joel Tellinghuisen, in *Excimer Lasers-1983*, edited by C. K. Rhodes, H. Egger, and H. Pummer (AIP Conference Proceedings Number 100, AIP, New York, 1983), p. 99. (Appendix 5)
8. "Mixed Representations for Diatomic Spectroscopic Data: Application to HgBr," by Joel Tellinghuisen and J. Gail Ashmore, Chem. Phys. Lett. (submitted -- Appendix 6)

Conference Papers - Cummulative Listing

1. "The B→X Transition in $^{200}Hg^{79}Br$," by J. Gail Ashmore and Joel Tellinghuisen, 37th Symposium on Molecular Spectroscopy (Columbus, Ohio), June, 1982.
2. "The B→X Transition in HgI," by K. S. Viswanathan and Joel Tellinghuisen, 37th Symposium on Molecular Spectroscopy (Columbus, Ohio), June, 1982.
3. "The Use of Morse-RKR Curves in Diatomic Calculations," by Stuart D. Henderson and Joel Tellinghuisen, 37th Symposium on Molecular Spectroscopy (Columbus, Ohio), June, 1982.
4. "Reanalysis of the B→X Transitions in the Mercury Halides," by J. Tellinghuisen, P. C. Tellinghuisen, J. G. Ashmore, and K. S. Viswanathan, 35th Gaseous Electronics Conference (University of Texas at Dallas), October, 1982.
5. "Spectroscopic Studies of Diatomic Electronic Transition Lasers," by Joel Tellinghuisen, 34th Southeastern Regional American Chemical Society Meeting (Birmingham, Alabama), November, 1982.
6. "The Emission Spectrum of HgI," by K. S. Viswanathan, O. Carlysle Salter, and Joel Tellinghuisen, 92nd Meeting of the Tennessee Academy of Science (Martin, Tennessee), November, 1982.
7. "The Emission Spectrum of HgBr," by J. Gail Ashmore and Joel Tellinghuisen, 92nd Meeting of the Tennessee Academy of Science (Martin, Tennessee), November, 1982.
8. "Interfacing a Microdensitometer to a Microcomputer," by O. Carlysle Salter and Joel Tellinghuisen, 92nd Meeting of the Tennessee Academy of Science (Martin, Tennessee), November, 1982.
9. "The Use of Morse-RKR Curves in Diatomic Calculations," by Stuart D. Henderson and Joel Tellinghuisen, 92nd Meeting of the Tennessee Academy of Science (Martin, Tennessee), November, 1982.
10. "Mercury Halide Spectroscopy," by Joel Tellinghuisen, Topical Meeting on Excimer Lasers (Incline Village, Nevada), January, 1983. (see Appendix 5)
11. " 'Best' Spectroscopic Constants for HgBr from Direct Fits of Multiple Band Systems to Polynomials and Near-Dissociation Expansions," by J. Gail Ashmore and Joel Tellinghuisen, 38th Symposium on Molecular Spectroscopy (Columbus, Ohio), June, 1983. (Appendix 7)
12. "Interfacing a Microdensitometer to a Microcomputer," by O. Carlysle Salter and Joel Tellinghuisen, 38th Symposium on Molecular Spectroscopy (Columbus, Ohio), June, 1983. (Appendix 7)

$B \rightarrow X$ transitions in HgCl and HgI

Joel Tellinghuisen, Patricia C. Tellinghuisen, Sue A. Davies, Patrick Berwanger, and K. S. Viswanathan
Department of Chemistry, Vanderbilt University, Nashville, Tennessee 37235

(Received 7 June 1982; accepted for publication 17 August 1982)

The $B \rightarrow X$ spectra of HgCl and HgI are studied at high resolution for the single isotopic species, $^{200}Hg^{35}Cl$, $^{200}Hg^{127}I$, and $^{200}Hg^{129}I$. For HgI the analysis indicates that the v'' numbering should be decreased by one unit from the previous assignment. For both molecules the analyses deviate progressively from the previous assignments at high v'', extrapolating to lower estimates of the ground-state dissociation energies. Franck–Condon calculations yield ΔR_e $(= R_e' - R_e'')$ $= 0.60$ Å for HgCl and 0.49 Å for HgI. The strongest laser features previously reported for HgCl occur near the heads of the overlapped 0–22, 1–23, 2–24, and 3–25 bands. The HgI laser operates in the region of the 0–14, 0–15, 1–15, 1–16, 2–17, and 2–18 bands.

PACS numbers: 33.20.Kf, 33.10.Gx, 33.70. – w, 42.55.Hq

In the search for new, high-power, UV-visible lasers, considerable attention has been focused on the $B \rightarrow X$ transitions in the diatomic mercury halides. To refine the spectroscopic characterization of these systems, we have been studying the emission spectra of isotopically pure HgX molecules. We reported recently preliminary results of our work on HgBr.[1] In this letter we discuss the results of our vibrational analyses for HgCl and HgI.

The emission spectra were obtained using equipment and procedures similar to those described previously.[1–4] The tesla discharge sources were charged initially with the desired isotopic HgX species, which were prepared *in situ* as described for HgBr.[1] Most of the work involved sources containing ^{200}Hg ^{35}Cl and ^{200}Hg ^{127}I. To determine the vibrational numbering we also photographed and measured spectra of ^{200}Hg ^{129}I ($^{129}I_2$ from Oak Ridge, stated isotopic purity 99%), and $^{200}Hg^{37}Cl$ (from a source made with natural Cl_2). HgCl spectra were photographed over the region 4400–5800 Å, at a reciprocal dispersion of ~5.3 Å/mm. The HgI spectra were recorded for the region 4050–4500 Å; most of the assignments were from plates having a reciprocal dispersion of ~1.1 Å/mm, with a few obtained from plates exposed at the lower resolution employed for HgCl.

As in the case of our earlier work on HgBr, our interpretation of the spectra of both molecules agrees qualitatively with Wieland's[5,6] previous work, except at the long-wavelength end. However, our least-squares analysis (see below) indicates that the v'' numbering suggested by Wieland for HgI should be decreased by one unit. (Wieland's numbering was stated to be uncertain for lack of a halogen isotope effect, since natural I_2 is 100% $^{127}I_2$.) Below $v'' = 14$ in HgI and $v'' = 20$ in HgCl, our measurements lie uniformly 2–3 cm^{-1} below Wieland's, which is consistent with the small isotope shift for ^{200}HgX versus the ^{202}HgX which dominated Wieland's spectra. However, for higher v'' our assignments deviate progressively to the blue of Wieland's, with the discrepancy amounting to 30 cm^{-1} for our highest presently assigned level ($v'' = 23$) in HgI, and about 40 cm^{-1} in HgCl ($v'' = 31$). As for HgBr, the relevant bands lie in very congested regions of the spectra and are likely blended to indistinction in spectra of "natural" HgCl and HgI. The assignments can be made with confidence in our single species spectra.

At present our assignments for ^{200}Hg ^{35}Cl include 39 bands spanning v' levels 0–9 and v'' levels 11–31. For HgI we have assigned 50 bands for ^{200}Hg ^{127}I and 54 for ^{200}Hg ^{129}I, spanning $v' = 0$–13 and $v'' = 5$–23. The assignments can be extended provisionally to higher v'' in both cases; however, the bands in question display anomalous profiles, requiring care in the estimation of band origins from the measured heads. Consequently, we are continuing to work on these regions. The assigned bands have been least-squares fitted to the standard double polynomials in $\rho(v' + 1/2)$ and $\rho(v'' + 1/2)$ [see Eqs. (1) and (2) in Ref. 1]. For HgI the variance increases by a factor of 2 when the v'' numbering is altered by ± 1 from our new numbering (which is reduced by one unit from Wieland's), so the new numbering is pre-

TABLE I. Spectroscopic parameters (cm^{-1}) for the $B \rightarrow X$ transitions in HgCl and HgI.[a]

	^{200}Hg ^{35}Cl[b]	^{200}Hg ^{127}I[c]
ΔT_e	23451.6	24066.4
$c_{v1}'(\omega_e')$	191.941	110.850
$c_{v2}'(-\omega_e x_e')$	−0.4754	−0.1716
$c_{v1}''(\omega_e'')$	298.973	123.053
$c_{v2}''(-\omega_e x_e'')$	−2.1513	−0.7130
c_{v3}''	1.0112×10^{-2}	-3.1161×10^{-2}
c_{v4}''	$-5.0^{c}62\times10^{-4}$	2.7567×10^{-4}
σ	0.37	0.19
$\mathscr{D}_e'$	39900[d]	38300[d]
$\mathscr{D}_e''$	8350	2900
R_e' (Å)	3.02	3.30
R_e'' (Å)	2.42	2.81
$c_{r1}'(B_e')$	0.06210	0.01994
$c_{r2}'(-\alpha_e')$	-2.1×10^{-4}	-4.2×10^{-5}
$c_{r1}''(B_e'')$	0.09674	0.02747
$c_{r2}''(-\alpha_e'')$	-7.239×10^{-4}	-1.954×10^{-4}
c_{r3}''	9.006×10^{-6}	-6.466×10^{-7}
c_{r4}''	-4.889×10^{-7}	-1.571×10^{-7}

[a] All rotational constants are intended as guidelines only, as they are based upon assumptions about the potential curves; see text.
[b] Vibrational constants valid for $v' = 0$–9, $v'' = 11$–31.
[c] Vibrational constants valid for $v' = 0$–13, $v'' = 5$–23.
[d] Assuming dissociation to $Hg^+(^2S) + X^-(^1S)$. The lowest $Hg^+ + X$ asymptote lies 17 400 cm^{-1} lower in HgCl and 21 800 cm^{-1} lower in HgI.

 0003-6951/82/090789-03$01.00

TABLE II. Isotopic ρ factors and abundances for isotopic species in HgCl and HgI.[a]

HgCl	Abundance	ρ	HgI	Abundance	ρ
198, 35	7.6%	1.000 752	198, 127	10.0%	1.001 961
199, 35	12.7	1.000 374	199, 127	16.8	1.000 975
200, 35	17.4	1.000 000	200, 127	23.1	1.000 000
201, 35	10.0	0.999 629	201, 127	13.2	0.999 032
202, 35	22.5	0.999 262	202, 127	29.8	0.998 074
204, 35	5.2	0.998 538	204, 127	6.9	0.996 181
198, 37	2.4	0.977 508			
199, 37	4.1	0.977 121			
200, 37	5.7	0.976 738			
201, 37	3.2	0.976 358			
202, 37	7.3	0.975 982			
204, 37	1.7	0.975 241			

[a] Reference molecules are $^{200}Hg\ ^{35}Cl$ and $^{200}Hg\ ^{127}I$.

ferred. For HgCl we have fitted only the bands measured for $^{200}Hg\ ^{35}Cl$. However, we have verified Wieland's numbering by measuring several prominent bands in the $v' = 0$ progression for $^{200}Hg\ ^{37}Cl$. In this case the effect of the change in the Cl mass is substantial, so that a change in the v'' numbering represents a $\sim 5\ cm^{-1}$ shift in the band positions. The agreement is within $1\ cm^{-1}$, in confirmation of Wieland's numbering.

Minimum variance was achieved in the least-squares fits using two upper state parameters and four lower state parameters for both molecules. The results are presented in Table I. The reader is cautioned not to trust these constants outside the v' and v'' regions spanned by the assignments. For example, the minimum of the X state remains uncertain by about $20\ cm^{-1}$ in HgCl, relative to the lowest assigned v'' level. However, within the sampled regions these constants should permit calculation of band positions reliable to about the standard deviations in the fits ($0.37\ cm^{-1}$ for HgCl, $0.19\ cm^{-1}$ for HgI). This reliability should extend to the other isotopic molecules, for which band positions can be calculated by substituting the appropriate isotopic ρ values in the polynomials. These ρ values are summarized in Table II. For reference we note that the isotopic shifts in the region of strong emission are about $1.1\ cm^{-1}$ per unit Hg mass change for HgI, and about $1.5\ cm^{-1}$ for HgCl.

We have attempted to estimate the dissociation energies for the X states of both molecules using long-range theory in the manner employed by Wilcomb and Bernstein.[7] However, in both cases we have encountered the same problem met in the work on HgBr: for our highest assigned levels the absolute slopes in the appropriate long-range plots are already *greater* than the theoretical limiting slopes. Consequently, we can presently give only rough upper bounds on $\mathcal{D}_0$ of $2850\ cm^{-1}$ and $8200\ cm^{-1}$ for HgI and HgCl, respectively. These values are 300–400 cm^{-1} lower than estimated by Wilcomb and Bernstein and in fact are close to the original estimates of Wieland.

Franck–Condon calculations corroborate our vibrational assignments and indicate that R_e' is larger than R_e'' by 0.60 Å in HgCl and 0.49 Å in HgI. In these calculations we took the approach used in the work on HgBr: we fixed the X curves at the R_e values used by Cheung and Cool[8] and varied the internuclear distance in the B states. The X curves were approximated as Morse/RKR curves,[9] and the B curves as Morse curves. The resulting R_e' values are thought to be reliable within 0.01 Å, relative to the X curves in the region for strong emission. For HgI our R_e' value is 0.03 Å larger than Cheung and Cool's. However, this distance is entirely due to a shift in the attractive branch of the X curve in the Franck–Condon region of strong emission; and with the change in the v'' numbering, our Franck–Condon distributions are in agreement with theirs. For HgCl our R_e' value is 0.08 Å larger than Cheung and Cool's. Most of this difference is significant, and it results in a shift of the Franck–Condon distributions upward by two v'' units (e.g., the FC gap for $v' = 1$ occurs near $v'' = 19$ instead of $v'' = 17$, as indicated in Table 8 of Ref. 8).

The R_e values are known in only a relative sense, as we have not yet analyzed rotational structure. However, preliminary examination of several strong bands in the $v' = 0$ progression for HgCl indicates that R_e' is ~ 3.00 Å in this molecule. This value is slightly smaller than the value in Table I but larger than Wadt's[10] theoretical estimate (2.93 Å). For HgBr the experimental estimate[11] is 3.06 Å, which is only 0.02 Å larger than the theoretical value.[10] Although the rotational constants for HgI and HgCl have not yet been determined experimentally, we include as guidelines in Table I the parameters calculated for the X curves employed in the Franck–Condon calculations.

Lasing has been reported for HgI at a number of wavelengths between 4414 and 4450 Å,[12–14] and for HgCl in the 5334–5658-Å region.[12,14–17] The laser features generally correspond to the most intense features in the spontaneous emission spectra and probably involve multipy overlapped rovibronic transitions in the several isotopic molecules of significance (see Table II). The prominent v'–v'' bands in the lasing region for HgI are 0–13, 0–14, 1–15, 1–16, 2–17, 2–18, 3–18, 3–19, 4–19, 4–20, 5–21, and 5–23. The strongest features in the HgCl laser spectrum occur near 5580 Å and undoubtedly involve appreciable contributions from transitions in the nearly coincident 0–22 and 1–23 bands, as has been noted previously. The 2–24 and 3–25 bands could also contribute significantly, as they lie very close to the other two and have large FCF's.

In a recent paper, Kvasnik and King[17] have measured and assigned 41 features in the HgCl laser spectrum. While

many of the listed features likely involve some of the indicated bands, we think it is unwise to make specific v'–v'' assignments for most of these lines, as they probably involve circumstantial overlap of rotational lines in several bands of the various isotopic molecules. Furthermore, Kvasnik and King's high-v'' assignments are inconsistent with our reanalysis of this transition. These authors also concluded that the HgCl emission in the 5540–5730-Å region includes a significant broadband contribution, attributed to a bound-free transition. We think it unlikely that such a bound-free transition could involve any of the known states of HgCl for the following reasons. (1) The $B \rightarrow A$ transition should lie about 4000 cm^{-1} to the red of $B \rightarrow X$. (2) The $C \rightarrow A$ and $D \rightarrow A$ systems *may* occur in this region; however, if these systems are present, the $C \rightarrow X$ and $D \rightarrow X$ systems should occur strongly in the UV. To our knowledge strong emission in the latter systems has not been reported for typical laser excitation conditions. (3) The continuum of the $B \rightarrow X$ transition falls precisely in this region; however, the Franck–Condon properties of this system prohibit significant continuous emission from v' levels less than 11. At a typical operating temperature of 150 °C the Boltzmann factor for the sum of *all* levels greater than 10 is about 10^{-3}. Thus if vibrational thermalization is appreciable, the $B \rightarrow X$ continuum must be negligible. While we cannot rule out broadband emission from other species in Kvasnik and King's laser system, we think it possible that their continuum is simply the quasicontinuum of densely overlapped lines in the $B \rightarrow X$ discrete emission. Even in our high-resolution, single-isotope spectra the emission appears almost continuous in some regions.

This work was supported by the Office of Naval Research.

[1]J. Tellinghuisen and J. G. Ashmore, Appl. Phys. Lett. **40**, 867 (1982).
[2]J. Tellinghuisen, Chem. Phys. Lett. **49**, 485 (1977).
[3]M. R. McKeever, A. Sur, A. K. Hui, and J. Tellinghuisen, Rev. Sci. Instrum. **50**, 1136 (1979).
[4]A. Sur, A. K. Hui, and J. Tellinghuisen, J. Mol. Spectrosc. **74**, 465 (1979).
[5]K. Wieland, Helv. Phys. Acta **14**, 420 (1941).
[6]K. Wieland, Z. Elektrochem. **64**, 761 (1960).
[7]B. E. Wilcomb and R. B. Bernstein, J. Mol. Spectrosc. **62**, 442 (1976).
[8]N. -H. Cheung and T. A. Cool, J. Quant. Spectrosc. Radiat. Transfer **21**, 397 (1979).
[9]J. Tellinghuisen and S. D. Henderson, Chem. Phys. Lett. (in press).
[10]W. R. Wadt, Appl. Phys. Lett. **34**, 658 (1979).
[11]J. G. Ashmore and J. Tellinghuisen, J. Mol. Spectrosc. (to be published).
[12]E. J. Schimitschek, J. E. Celto, and F. Hanson (unpublished).
[13]Yu. E. Gavrilova, V. S. Zrodnikov, A. D. Klementov, and A. S. Podsosonny, Sov. J. Quantum Electron. **10**, 1457 (1980).
[14]R. Burnham, Appl. Phys. Lett. **33**, 156 (1978).
[15]J. H. Parks, Appl. Phys. Lett. **31**, 192 (1977).
[16]K. Y. Tang, R. O. Hunter, Jr., J. Oldenettel, C. Howton, D. Huestis, D. Eckstrom, B. Perry, and M. McCusker, Appl. Phys. Lett. **32**, 226 (1978).
[17]F. Kvasnik and T. A. King, Opt. Commun. **41**, 199 (1982).

Appendix 2

THE USE OF MORSE–RKR CURVES IN DIATOMIC CALCULATIONS

Joel TELLINGHUISEN and Stuart D. HENDERSON
Department of Chemistry, Vanderbilt University, Nashville, Tennessee 37235, USA

Received 12 July 1982

The potential curves for diatomic states which have known vibrational constants but unknown rotational constants can be approximated well by a combination Morse–RKR curve. The approximation is tested on 25 well-known potentials.

1. Introduction

The emission and absorption spectra of heavy diatomic molecules are usually rotationally and vibrationally congested. For a particular electronic transition it is often possible to obtain a reliable vibrational analysis, but difficult or nearly impossible to achieve a rotational analysis. By way of example, this situation holds for most of the halogen, rare-gas halide, and mercury halide emission systems studied in our laboratory in recent years, even though our experimental resolution is moderately high [$(1-2)\times10^5$]. For the calculation of important properties of the transition, such as Franck–Condon factors and band shapes, one can have potential curves for both electronic states. The standard procedure for obtaining such curves is the RKR method. However, in the absence of rotational constants the RKR method can yield only the width of the potential, $R_+ - R_-$, as a function of v and G_v. Thus to obtain a suitable potential in such cases it is necessary to *guess* the equilibrium internuclear distance and the shape of either the inner or outer branch of the potential.

In this situation we have often approximated the unknown repulsive or inner branch (R_-) by a Morse potential, then simply added the RKR width as a function of energy to obtain the attractive or outer branch (R_+). We will call such potentials Morse–RKR potentials. In the present work we have tested this approximation on 25 potentials which are well known over a significant fraction of the well depth. We find that the Morse curve is a surprisingly good representation of the inner branch of the potential, with errors in R_- typically less than 0.02 Å near the dissociation limit, and seldom more than 1% of R_e.

2. Theory

The Morse curve is one of the simplest of "realistic" diatomic potentials, requiring only three parameters for specification [1],

$$U(R) = \mathcal{D}_e[1 - e^{-\beta(R-R_e)}]^2 , \tag{1}$$

where R_e is the equilibrium internuclear distance and $\mathcal{D}_e$ the dissociation energy. The parameter β (units $Å^{-1}$) is given by

$$\beta = 0.121777\ \omega_e(\mu/\mathcal{D}_e)^{1/2} , \tag{2}$$

where ω_e (the vibrational frequency) and $\mathcal{D}_e$ are in units cm^{-1}, and the reduced mass μ is in amu. Because of the relation, $\mathcal{D}_e = \omega_e^2/4\omega_e x_e$, eq. (2) may also be written,

$$\beta = 0.243555\ (\mu\omega_e x_e)^{1/2} . \tag{3}$$

The RKR method [2] involves evaluation of the integrals,

$$2f = a\int_{v_{min}}^{v} (G_v - G_{v'})^{-1/2}\,dv' = R_+ - R_- , \tag{4}$$

0 009-2614/82/0000–0000/$ 02.75 © 1982 North-Holland

$$2g = a^{-1}\int_{v_{min}}^{v} B_{v'}(G_v - G_{v'})^{-1/2}\,dv' = R_-^{-1} - R_+^{-1} , \tag{5}$$

where the constant a contains the reduced mass, G_v is the vibrational energy, and B_v is the rotational constant. Through the f and g integrals, the turning points are determined as a function of v and G_v.

The Klein f and g integrals contain a singularity at the upper limit of integration, which, however, can be treated effectively a number of ways (e.g. refs. [3,4]). Consequently the turning points can be calculated with very high numerical accuracy. The RKR method is a semiclassical method; nonetheless it typically gives quantum mechanical consistency within $\approx 1\ cm^{-1}$, even in the first-order form of eqs. (4) and (5). Note that the f integral, which determines the width of the potential, involves the vibrational constants alone. Thus if one branch, say R_-, is known, only the vibrational constants are needed to calculate the other (R_+). This point has been realized and taken advantage of by a number of authors in various applications.

It is well known that the Morse curve and indeed many other 3–5-parameter functions do a good job of approximating the low-lying rovibrational levels of most bound diatomic states [5]. However, all such closed-form potentials become progressively less reliable with increasing energy and may show errors of $10^3\ cm^{-1}$ in the energy as a function of R in both the inner and the outer branch, as compared with the true (RKR) curve. However, the errors in the inner branch may be less significant than they appear, because the potential is very steep on its inner wall. Hence, we pose the question differently: What is the *error in R_- as a function of the energy*? For the purpose of calculating Franck–Condon factors (FCFs), approximate rotational and centrifugal distortion constants, and band contours, the error in $R_-(U)$ is really the quantity of direct interest, because in first approximation the effect of such an error is a simple translation of the wavefunction by ΔR_- from its true position. Stated differently, two potentials which have different R_- curves but the same width as a function of energy, will have identical semiclassical eigenvalues and nearly identical quantum eigenvalues for $J = 0$. The wavefunctions will be similar in appearance in the two cases, but skewed in position for one relative to the other. For $J > 0$ the eigenvalues and wavefunctions will of course not be the same for the two curves.

As a function of the potential energy U the Morse turning points are given by

$$R_\pm = R_e - \beta^{-1}\ln[1 \mp (U/\mathcal{D}_e)^{1/2}] . \tag{6}$$

3. Calculations

We have compared the Morse and RKR repulsive branches for 25 reasonably well-known diatomic potentials, ranging in bond energy from one of the weakest [NaAr(X): $\mathcal{D}_e = 40.4\ cm^{-1}$] to the strongest [CO(X): $\mathcal{D}_e = 90540\ cm^{-1}$]. Most of these potentials are for ground states, but a few excited states are included, also. In all but one case the spectroscopic constants (and hence the RKR curve) are reliable for more than half the well depth; in most cases the range of validity extends beyond 80% of $\mathcal{D}_e$. The results are summarized in table 1. Typical good and bad performances of the Morse approximation are illustrated in figs. 1 and 2.

From these calculations we make the following observations:

(1) In all but seven cases the Morse curve defined by the experimental ω_e and $\omega_e x_e$ values agrees better with the RKR curve than does the Morse curve defined by the experimental ω_e and $\mathcal{D}_e$. In six of the exceptions, however, the differences in the two Morse curves are insignificant; and in the other [$I_2(A)$], it is likely that the experimental $\omega_e x_e$ value is not yet very well defined.

(2) The maximum relative errors ($\Delta R_-/R_e$) obtained using the Morse curve defined by ω_e and $\omega_e x_e$ exceed 1% in only six cases, one being the aforementioned A state of I_2, the others being states in H_2 and the alkali dimers.

(3) The worst agreement is obtained for XeCl(X). This state is somewhat anomalous, and the shape of its curve is known only through trial-and-error Franck–Condon calculations, not from a rotational analysis. Of the others, $H_2(X)$ stands out as an example of particularly poor agreement.

(4) In almost every case the calculated $\mathcal{D}_e$ value is larger than the experimental value. Omitting the anomalous A state of I_2 and the four van der Waals molecules, the $\mathcal{D}_e'/\mathcal{D}_e$ ratio averages 1.34 with a

Table 1
Summary of Morse calculations for selected potentials. RKR curves were either taken from, or calculated from constants given in the indicated references. All spectroscopic constants are in units cm^{-1} and Å.

State	R_e	ω_e	$\omega_e x_e$	$\mathcal{D}_e$ [a]	$\mathcal{D}_e / \mathcal{D}_e$ [a]	β [a]	β' [a]	Range [b]	$\Delta R_-/R_e$ [c] ($\times 10^3$)		Ref.
$H_2(X)$	0.741	4401.21	121.34	38.300	1.04	1.9436	1.9039	0.92	−34	−37	[6]
$Li_2(X)$	2.673	351.42	2.583	8.620	1.39	0.8636	0.7331	0.53	11	3	[7]
$Li_2(A)$	3.108	255.47	1.582	9.450	1.09	0.5994	0.5736	0.58	−8	−11	[7]
$Na_2(X)$	3.079	159.11	0.721	5.990	1.47	0.8489	0.7014	0.91	25	12	[8]
$Na_2(B)$	3.413	124.44	0.760	3.120	1.63	0.9204	0.7198	0.91	23	9	[8]
$K_2(X)$	3.905	92.02	0.283	4.190	1.79	0.7639	0.5718	0.59	24	12	[9]
$Cs_2(X)$	4.650	42.02	0.082	3.550	1.52	0.7001	0.5684	0.67	25	16	[10]
$N_2(X)$	1.098	2358.57	14.324	79.890	1.22	2.6888	2.4391	0.55	4	−1	[11]
$N_2(A)$	1.287	1460.64	13.872	29.690	1.30	2.7320	2.4006	0.58	5	0	[11]
CO(X)	1.128	2169.81	13.288	90.540	0.98	2.2994	2.3247	0.82	−4	1	[12]
SiO(X)	1.510	1241.56	5.966	67.240	0.96	1.8600	1.8978	0.55	−3	−4	[13]
$O_2(X)$	1.208	1580.19	11.981	42.050	1.24	2.6539	2.3841	0.71	2	−4	[14]
$O_2(A)$	1.522	799.08	12.16	6.650	1.97	3.3748	2.4018	0.98	14	3	[14]
$O_2(B)$	1.604	709.06	10.65	8.120	1.46	2.7097	2.2439	0.90	14	6	[14]
$S_2(X)$	1.889	725.65	2.844	35.240	1.31	1.8821	1.6422	0.63	3	−2	[13]
$Se_2(X)$	2.166	385.30	0.964	27.700	1.39	1.7820	1.5113	0.39	3	−1	[13]
$Cl_2(X)$	1.988	559.75	2.694	20.280	1.43	2.0017	1.6716	0.99	8	0	[15]
$I_2(X)$	2.666	214.55	0.619	12.550	1.48	1.8580	1.5264	0.98	9	2	[16]
$I_2(A)$	3.118	94.96	2.43	1.640	0.57	2.2745	3.0245	0.95	9	17	[17,18]
$I_2(A')$	3.080	108.81	1.283	2.510	0.92	2.1212	2.1975	0.98	7	8	[19,20]
$I_2(B)$	3.027	125.67	0.753	4.380	1.20	1.8488	1.6832	0.99	10	6	[21]
$Ar_2(X)$	3.759	31.33	2.899	99.6	0.85	1.7095	1.8537	1.02	0	3	[22]
$Mg_2(X)$	3.889	51.08	1.623	430	0.93	1.0388	1.0746	0.97	−10	−8	[23]
NaAr(X)	4.994	13.56	1.155	40.4	0.99	0.9922	0.9999	1.29	6	6	[24]
XeCl(X)	3.23	26.22	−0.321	281	–	1.0050	–	0.95	−76	–	[25]

[a] Unprimed quantities refer to the experimental $\mathcal{D}_e$ and values calculated therefrom; primes denote quantities calculated from the experimental ω_e and $\omega_e x_e$.
[b] Range of validity of known potential, as a fraction of the well depth.
[c] ΔR_- is defined as R_-(Morse) − R_-(RKR). The tabulated values are the maximum errors. First entry is for the Morse curve defined by $\mathcal{D}_e$ and β, second for $\mathcal{D}'_e$ and β'.

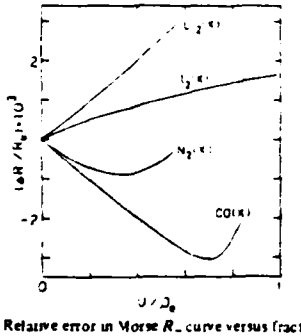

Fig. 1. Relative error in Morse R_- curve versus fractional binding energy for $Li_2(X)$, $I_2(X)$, $N_2(X)$, and CO(X).

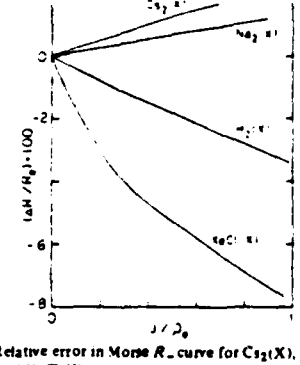

Fig. 2. Relative error in Morse R_- curve for $Cs_2(X)$, $Na_2(X)$, $H_2(X)$, and XeCl(X).

standard deviation of 0.27. For the "single-bonded" ground states (seven cases), this ratio is still higher, 1.45 ± 0.22. If the A and A' states of I_2 are recalculated using $\mathcal{D}_e$ values 40% larger than the experimental values, the maximum relative errors drop to 0.005 and 0.003, respectively.

(5) The calculated β' values span a fairly narrow range from 0.57 to 2.44 $Å^{-1}$ (excluding the A state of I_2). The smallest values occur for the "soft" alkali potentials, the largest for the doubly and triply bonded states. Note that the small range for β can be related to the fact that this parameter has no dependence on the reduced mass. This is evident from eq. (3), since for a given potential, $\omega_e x_e$ contains an inverse μ dependence [1].

4 Discussion

For most of the examined cases, the maximum error in R_- is less than 1%, which translates into a skewedness error of typically 0.01–0.03 Å. This figure is comparable to the precision obtainable in the trial-and-error FCF and band profile calculations mentioned earlier [17,19]. Thus, to the extent that the examined potentials are representative of all bound diatomic potentials, it would appear that the Morse approximation for the repulsive branch is at least a good "bet" for a state having unknown or poorly defined rotational constants. Accordingly the errors in the FCF calculations due to uncertainties in the *shape* of the potential so defined are not likely to be large. (Of course the Morse curve can offer no guidance for guessing R_e.) If possible, the experimental ω_e and $\omega_e x_e$ values should be used to define the Morse R_- curve. In those cases where ω_e and $\mathcal{D}_e$ are approximately known, but $\omega_e x_e$ is poorly defined, we recommend use of a $\mathcal{D}_e$ value 40% greater than the experimental value.

Regarding the representativeness of the chosen potentials, we can only say that we have not held back any results (i.e. we have examined only the 25 states of table 1); and to select these we have used only the criteria of ready availability and a reasonably large range of energy over which the experimental constants are valid. We have not tried potentials other than the Morse curve, some of which likely perform as well or better. However, the Morse curve is easy to use and appears to be adequate for the applications we have mentioned.

From the reasonably good agreement between the Morse and RKR R_- curves, one might naturally wonder how reliably the α_e constants can be predicted from the Morse expression [1].

$$\alpha_e = (6B_e^2/\omega_e)\,[(\omega_e x_e/B_e)^{1/2} - 1]. \qquad (7)$$

Indeed for the states of table 1 (omitting XeCl(X) and I_2(A)), we find an average absolute error of 13% and an average signed error of 6% in the α_e values calculated from eq. (7). If the three worst cases (H_2(X), Cs_2(X), K_2(X)) are excluded, these figures drop to 9 and 3%, respectively. However, this agreement should not be taken as justification for using a two-term Morse expression for B_v, except for low v: because (a) unlike the G_v expression, the B_v expression for a Morse curve does not terminate with two terms, and (b) the B_v values for the Morse–RKR curve will anyway be different from the Morse values. For high v levels the Morse–RKR B_v values must be evaluated numerically, from R^{-2} expectation values.

There is one other approach to this problem of "guessing half a potential" which we have used with success [19,26], namely Jenc's reduced potential curve (RPC) method [27]. As Jenc showed years ago, the concept of a single RPC has some validity for "analogous" potentials. We have found that this is particularly true of the repulsive branches, and we have used Jenc's method to guess the shapes of the potentials for the Cs_2(X) [26] and I_2(A') states [19]. Subsequent work by others [10,20] has shown that, with a shift in R_e, our guessed potentials are very close to the true curves. For example, our R_- branch for I_2(A') [19] differs from the recently determined RKR curve [20] by 0.031 Å over the entire range of validity of our constants. We have calculated the RPCs for the states of table 1 and found, in agreement with Jenc's earlier work, that for such a range of states there is no adequate single RPC. In fact the scatter in the RPC R_- curves is considerably greater than in the Morse calculations. Hence the RPC method should be reserved for states which can reasonably be treated as analogues of other, better known states.

Acknowledgement

This work was supported by the Office of Naval Research.

References

[1] G. Herzberg, Spectra of diatomic molecules (Van Nostrand, Princeton, 1950).
[2] O. Klein, Z. Physik 76 (1932) 226.
[3] J. Tellinghuisen, J. Mol. Spectry. 44 (1972) 194.
[4] H. Telle and U. Telle, J. Mol. Spectry. 85 (1981) 248.
[5] D. Steele, E.R. Lippincott and J.T. Vanderslice, Rev. Mod. Phys. 34 (1962) 239.
[6] T.E. Sharp, At. Data 2 (1971) 119.
[7] P. Kusch and M.M. Hessel, J. Chem. Phys. 67 (1977) 586.
[8] P. Kusch and M.M. Hessel, J. Chem. Phys. 68 (1978) 2591.
[9] W.J. Tango, J.K. Link and R.N. Zare, J. Chem. Phys. 49 (1968) 4264.
[10] G. Honing, M. Czajkowski, M. Stock and W. Demtroder, J. Chem. Phys. 71 (1979) 2138.
[11] A. Lofthus and P.H. Krupenie, J. Phys. Chem. Ref. Data 6 (1977) 113.
[12] A.W. Mantz, J.-P. Maillard, W.B. Roh and K. Narahari Rao, J. Mol. Spectry. 57 (1975) 155.
[13] K.P. Huber and G. Herzberg, Constants of diatomic molecules (Van Nostrand, Princeton, 1979).
[14] P.H. Krupenie, J. Phys. Chem. Ref. Data 1 (1972) 423.
[15] A.E. Douglas and A.R. Hoy, Can. J. Phys. 53 (1975) 1965.
[16] J. Tellinghuisen, M.R. McKeever and A. Sur, J. Mol. Spectry. 82 (1980) 225.
[17] K.S. Viswanathan, A. Sur and J. Tellinghuisen, J. Mol. Spectry. 86 (1981) 393.
[18] S. Gerstenkorn, P. Luc and J. Verges, J. Phys. B 14 (1981) L193.
[19] J. Tellinghuisen, J. Mol. Spectry. 94 (1982), to be published.
[20] J.B. Koffend, A.M. Sibai and R. Bacis, J. Phys. (Paris), to be published.
[21] P. Luc, J. Mol. Spectry. 80 (1980) 41.
[22] E.A. Colbourn and A.E. Douglas, J. Chem. Phys. 65 (1976) 1741.
[23] C.R. Vidal and H. Scheingraber, J. Mol. Spectry. 65 (1977) 46.
[24] J. Tellinghuisen, A. Ragone, M.S. Kim, D.J. Auerbach, R.E. Smalley, L. Wharton and D.H. Levy, J. Chem. Phys. 71 (1979) 1283.
[25] A. Sur, A.K. Hui and J. Tellinghuisen, J. Mol. Spectry. 74 (1979) 465.
[26] J. Tellinghuisen and M.B. Moeller, Chem. Phys. 50 (1980) 301.
[27] F. Jenc, J. Chem. Phys. 47 (1967) 127.

Direct fitting of spectroscopic data to near-dissociation expansions: $I_2(D' \rightarrow A')$, $Br_2(D' \rightarrow A')$, and XeCl($B \rightarrow X$ and $D \rightarrow X$)

Joel Tellinghuisen

Department of Chemistry, Vanderbilt University, Nashville, Tennessee 37235
(Received 13 October 1982; accepted 5 November 1982)

The utility of near-dissociation expansions (NDEs) for diatomic vibrational energies is tested through least-squares fitting of vibrational bandhead data for selected electronic transitions in I_2, Br_2, and XeCl. In these test cases, the NDEs show efficiency comparable to that for the traditional polynomials in $(v + 1/2)$. For data sets which span an intermediate range of v levels, the NDEs are clearly superior to the polynomials for extrapolating to higher v, and of comparable reliability in extrapolation to low v. However, in their approach to dissociation, the NDEs can show unphysical behavior, the correction of which requires further constraints on the form of the NDE. Also, for lengthy extrapolations the NDEs may yield optimistically precise yet erroneous values for the dissociation energy. The present best estimates of the dissociation energies ($\mathfrak{D}_e$) for the lower states involved in these calculations are 2506.0(3) cm^{-1} for $I_2(A')$, 2828(8) cm^{-1} for $Br_2(A')$, and 281.1(7) cm^{-1} for XeCl(X).

INTRODUCTION

Prior to 1970 the standard procedure for estimating iatomic dissociation energies from spectroscopic data 'as the Birge–Sponer (BS) extrapolation,[1,2] in which a lot of $\Delta G_{v+1/2}$ vs v is extended linearly to intercept the axis. The area under the extrapolated curve is then dded to the energy of the highest observed level to ield an estimate of $\mathfrak{D}_e$. A linear BS extrapolation is igorously correct for one of the simplest "realistic" iatomic potentials—the Morse curve. However, "real" iatomics do not follow Morse behavior near dissocia- ion; consequently, the BS plot is inherently curved. ince the BS method contains no prescription for esti- ating the curvature, the resulting estimates of $\mathfrak{D}_e$ may e very uncertain.

To remedy this deficiency, LeRoy and Bernstein[3,4] sed semiclassical theory to develop new extrapolation ethods based on the asymptotically limiting inverse ower potential,

$$V(R) = \mathfrak{D} - C_n/R^n \ . \tag{1}$$

fuch of the early work with these methods focused on he determination of $\mathfrak{D}$ and C_n for states for which spec- roscopic data were available close to the dissociation imit.[5] In such applications long-range methods yielded ery precise estimates of $\mathfrak{D}$, and C_n values which were ostly in fair agreement with theoretical values calcu- ated for the interacting atoms.

As it turns out, the long-range limiting behavior is ot very sensitive to errors in C_n. Taking advantage f this fact, Tellinghuisen *et al.*[6] and Wilcomb and ernstein[7] employed a variant method, in which C_n was xed at its theoretical value, to estimate $\mathfrak{D}$'s from data hich required long extrapolations. In a recent paper eRoy and Lam[8] have taken this idea further, using non- inear least-squares fits to expressions having the cor- ect limiting behavior at dissociation, with values of and C_n again fixed by theory.

In the present work I have expanded on the method of LeRoy and Lam[8] in a test of direct fitting of band- head data to near-dissociation expansions. Since all spectroscopic data represent energy *differences*, direct fits of raw data to expressions which include the energy levels for all involved states are preferred over methods which attempt to isolate the dependences on the different states through preliminary manipulation of the raw data. The latter, which include combination difference and term value methods, introduce bias and correlation error into the final results.[9,10] In the treatment of $BeAr^+$ by LeRoy and Lam,[8] the fitted energy levels were already a step removed from the raw data of Subbaram *et al.*[11] In the present case I have fitted bandhead data of electronic emission transitions in I_2, Br_2, and XeCl. These transitions all involve low v' levels, so the tra- ditional polynomial in $(v' + \frac{1}{2})$ is used to represent G'_v in each case. For XeCl the data sample a large fraction of the ground state; for I_2 and Br_2 an intermediate range of v'' is sampled. In the calculations I have focused my attention on the following question: How do (1) the efficiency and (2) the extrapolating ability of the near- dissociation expansions compare with those of the con- ventional polynomials? The results are generally fav- orable for the long-range method on both counts; how- ever, some limitations are noted.

II. THEORY

Near the dissociation limit the vibrational energy fol- lows the expression,[8]

$$G_v = \mathfrak{D}_e - X_n(v_D - v)^{2n/(n-2)} \ , \tag{2}$$

where v_D is the effective vibrational quantum number at dissociation, n is the theoretically appropriate inverse power of $R (n \leq 6)$, and the constant X_n contains the de- pendence on C_n and the reduced mass μ,

$$X_n = \bar{X}_n [\mu^n C_n^2]^{1/(2-n)} \ . \tag{3}$$

Values for the constant $\bar{X}_n$ for various n may be found in Ref. 8.

A different version of Eq. (2) is

 0021-9606/83/052374-07$2.10

$$dG_v/dv = K_n(\mathfrak{D}_e - G_v)^{(n+2)/2n} \quad , \tag{4}$$

where[6] $K_n = [2n/(n-2)] \times X_n^{(n-2)/2n}$. A modified form of Eq. (4),

$$g \equiv (dG_v/dv)^{2n/(n+2)} = K_n^{2n/(n+2)}(\mathfrak{D}_e - G_v) \, , \tag{5}$$

was employed in the graphical extrapolation methods of Refs. 6 and 7.

LeRoy and Lam[8] suggested the fitting of G_v values to an empirical extension of Eq. (2),

$$G_v = \mathfrak{D}_e - X_n(v_D - v)^{2n/(n-2)} F(v) \quad , \tag{6}$$

in which the correct limiting behavior is assured by designing the function $F(v)$ to go to unity as $v \to v_D$. The two functions examined in Ref. 8 were

$$F_{a,m}(v) = 1 + \sum_{i=1}^{m} a_i (v_D - v)^i \tag{7}$$

and

$$F_{b,m}(v) = \left[1 + \sum_{i=1}^{m} b_i (v_D - v)^i \right]^{2n/(n-2)} \quad . \tag{8}$$

In Eqs. (7) and (8) the $\{a_i\}$ and $\{b_i\}$ are purely empirical quantities to be determined from a fit of the data. In further work on rotational and centrifugal distortion constants, Tromp and LeRoy[12] have employed exponentials for $F(v)$. In the present work I have used only the F's of Eqs. (7) and (8) or simple modifications thereof.

For the four band systems investigated here, previous work has shown that two vibrational constants are adequate to represent the v' levels. Thus the data are fitted to expressions of the form,

$$\nu(v', v'') = T + G'_v + X_n(v_D - v'')^{2n/(n-2)} F(v'') \quad , \tag{9}$$

where $G'_v = \omega'_e(v' + \frac{1}{2}) - \omega_e x'_e(v' + \frac{1}{2})^2$. Note that the parameter T represents the energy difference between the minimum of the upper state and the dissociation limit of the lower state; in conventional polynomial fitting the corresponding term is ΔT_e.

The nonlinear fits were carried out using standard methods.[10,13] In particular the bookkeeping was greatly facilitated by use of the coefficient matrix U, which contains m columns (one for each adjustable parameter) and n rows (one for each experimental point).[10] In these nonlinear fits the elements of the ith row of this matrix are the partial derivatives of the fit function with respect to the parameters, evaluated at the ith point using the current estimates of the parameters. The corrections to the parameters are then calculated straightforwardly upon inverting the matrix $\mathbf{U}^T\mathbf{U}$; and the procedure is repeated until convergence is obtained.[13] Variable weights are readily accommodated.

Also of interest are the errors in the function and in other, derived functions of the parameters. The errors are calculated from the variance–covariance matrix [which is proportional to $(\mathbf{U}^T\mathbf{U})^{-1}$], using methods such as those described in Refs. 13 and 14. The quantities of particular interest are

$$\Delta T_e = \nu(-0.5, -0.5) \tag{10}$$

and

$$\mathfrak{D}''_e = \nu(v', -0.5) - \nu(v', v''_D) \quad . \tag{11}$$

III. RESULTS AND DISCUSSION

A. I_2 ($D' \to A'$)

I have recently reported a detailed vibrational analysis of the $D'(2g) - A'(2u)$ system (~ 3400 Å) of I_2,[15] with ~ 250 assigned bands for $^{127}I_2$ and $^{129}I_2$, spanning v' levels 0–15 and v'' levels 4–30. By identifying the D' state as the α state of King *et al.*,[16] I was able to estimate that $\mathfrak{D}_e$ for the A' state is very close to 2500 cm^{-1}. In more recent work Koffend *et al.*[17] have achieved a complete vibrational and rotational analysis of the A' state. Their work corroborates my assignment of the emission spectrum and yields precise information for v'' levels 0–59. Thus this system makes an interesting test for fitting to near-dissociation expansions (NDEs).

Data for multiple isotopic molecules can be readily accommodated in fits to Eq. (9), just as they can in conventional polynomial fitting. However, the vibrational numbering of the A' state is now certain, so data for multiple isotopes are not needed. Hence I have fitted only the $^{127}I_2$ bands in Table I of Ref. 15, with their associated weights.

For the A' state $n = 5$. For C_5 I have used the value $C_5 = 2.64 \times 10^5$ cm^{-1} Å^5, given by Mulliken[18] and used in Ref. 15. To obtain initial estimates of the parameters I used linearized versions of Eqs. (7)–(9). In this regard it is worth noting that $F_{a,m}(v)$ and variants thereof, with selected powers of $(v_D - v)$ omitted, are particularly convenient, since with v_D fixed, the fits to Eq. (9) become linear (which means that convergence occurs in one pass). For comparison with the NDE fits, I have also redone the polynomial fits for the $^{127}I_2$ data alone.

The results of these calculations are summarized in Table I. In the polynomial fits three constants were clearly inadequate for the A' state, and the most efficient representation was the $P_{2,4}$ fit (i.e., two upper- and four lower-state parameters, plus ΔT_e). In the NDE fits the number of parameters ranged from six to eight; in each case two vibrational constants were used for the upper state. The six-parameter NDE fits actually outperformed the six-parameter polynomial fit. However, the variances for the seven-parameter NDE fits were noticeably higher than that for the $P_{2,4}$ fit. In fact I was unable to make the nonlinear $F_{a,3}$ and $F_{b,3}$ fits converge. However, by treating v_D as a known, then varying it externally, I was able to find a minimum variance with respect to v_D. To calculate the errors in the nonlinear fits, I then simply froze the parameters at the values determined from optimization with respect to v_D. The instability in the seven-parameter NDE fits was manifested as large errors in and correlation between T and v_D. The $F_{a,4}$ fit also failed to converge, and in this case the minimum variance with respect to a "known" v_D occurred at the unrealistically large value $v_D \approx 228$, at which point T went to zero. Somewhat surprisingly the variance in this fit matched

TABLE I. Summary of various least-squares fits for the I_2 $D' \rightarrow A'$ system.[a]

Fit[b]	(σ^2)[c]	ΔT_e[d]	ω'_e	$\omega_e x'_e$	$\mathfrak{D}''_e$[d]	v''_D
$P_{2,3}$	0.669	30 367.2(1.7)	103.99(9)	0.210(8)	...	...
$P_{2,4}$	0.102	340.1(1.2)	4.00(4)	0.210(3)	...	...
$P_{2,5}$	0.101	337.4(2.7)	3.99(4)	0.209(3)	...	...
$P_{3,4}$	0.102	340.0(1.3)	4.06(7)	0.224(14)	...	...
$P_{3,5}$	0.102	337.8(2.7)	4.04(7)	0.222(14)	...	...
$F_{a,2}$	0.462	357.7(1.9)	4.05(8)	0.213(6)	2373(6)	63.4(2)
$F_{a,3}$	0.262	348.0(5.1)	4.02(6)	0.211(5)	2516(890)	82(142)
$F_{a,4}$	0.101	335.5(1.4)	3.98(4)	0.209(3)	...	...
$F_{b,2}$	0.472	358.4(1.9)	4.05(8)	0.213(6)	2372(6)	63.3(3)
$F_{b,3}$	0.245	346.2(5.6)	4.02(6)	0.211(5)	2538(2598)	90(905)
$F_{a,2}$*	0.483	358.3(2.0)	4.05(8)	0.214(6)	2364(6)	61.6(2)
$F_{a,3}$*	0.229	346.1(4.7)	4.02(6)	0.211(5)	2545(793)	81(97)

[a]All quantities in cm^{-1} except $\sigma^2(cm^{-2})$ and v_D (dimensionless).
[b]$P_{i,j}$ refers to polynomial fit having i upper-state parameters, j lower-state parameters, plus ΔT_e.
[c]Defined as $[(\Sigma w_i \delta v_i^2)/(\Sigma w_i)] \times [n/(n-m)]$, where w_i and δv_i are the weight and residual of the ith point, n is the number of data points, and m is the number of parameters.
[d]Current best estimates, $\Delta T_e = 30\,347.0\,cm^{-1}$, $\mathfrak{D}'_e = 2506.0\,cm^{-1}$; see Ref. 18.
*Fits for altered C_5 value; see the text.

that of the best polynomial fit! However, the NDE parameters were physically meaningless.

In all fits the vibrational parameters for the D' state were well determined and mutually consistent. Furthermore the estimates of ΔT_e from the NDE fits were close to those from the polynomials and showed comparable scatter and precision. In fact the values from the seven-parameter fits are very close to my current *best estimate*, $30\,347.0\,cm^{-1}$, obtained by correcting my results[15] in accord with the better definition of the A' state in Ref. 17.[18]

Some of these results are displayed in Fig. 1, which is the plot suggested by Eq. (15) and used previously in my laboratory for graphical estimation of $\mathfrak{D}_e$. I have included also the points calculated from the tabulated energy levels given in Ref. 17, using $dG_v/dv \approx (G_{v+1} - G_{v-1})/2$. The latter points diverge from my polynomial results above $v'' = 25$, suggesting that my assignments for $v'' > 25$ may be in error. When I dropped the questionable bands from the data set, the variances in the nonlinear fit to $F_{a,3}$ indeed dropped by a factor of 2; however the convergence problem persisted. From the data of Ref. 17 it is clear that the jog in the curve near $v = 23$ is real, even though my data may overemphasize it. This points up a limitation inherent in any attempt to estimate $\mathfrak{D}_e$ from data which are far from dissociation. There is clearly no way for any least-squares fit to correctly predict this type of behavior from data which do not sample the relevant region. In fact below $v = 22$ the data in Fig. 1 appear to follow the calculated limiting slope very nicely; lacking data above $v = 22$, one would estimate a $\mathfrak{D}_e$ value which is much below the true value and optimistically precise.

Another intersting point about the NDE results in Fig. 1 is that even though they are constrained to have the correct limiting behavior, the seven-parameter fits appear *not* to approach dissociation with the correct slope. In fact they *do*, but only very near v_D. This point is discussed further below, in conjunction with the Br_2 calculations.

To eliminate model dependence in the estimates of $\mathfrak{D}_e$ and v_D, LeRoy and Lam[8] took weighted averages of the various estimates, with weights proportional to the reciprocal variances of the individual estimates. In the present case this procedure would mean that the values are almost entirely determined by the six-parameter

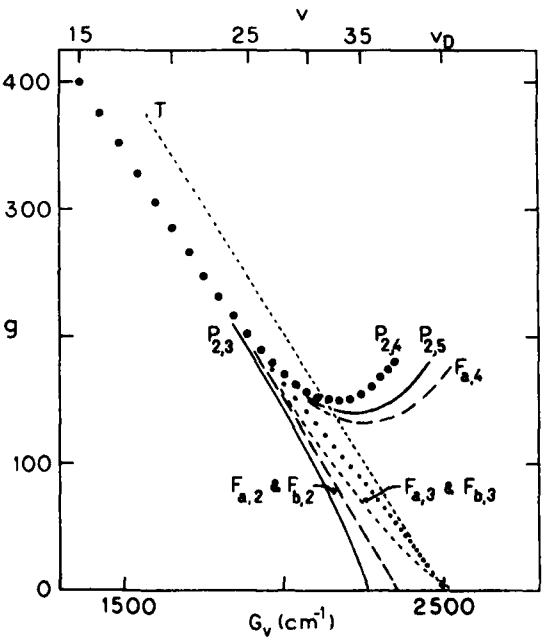

FIG. 1. Plots of g (units $cm^{-10/7}$) vs G_v for the $A'(2u)$ state of I_2. The large points are results from the $P_{2,4}$ polynomial fit; the small points are from results of Ref. 17. Also shown are the curves calculated from the results of two other polynomial fits and five near-dissociation fits. The limiting theoretical behavior is indicated by the dashed line (T). All calculated g curves have their G_v scales adjusted to be coincident at $v = 20$.

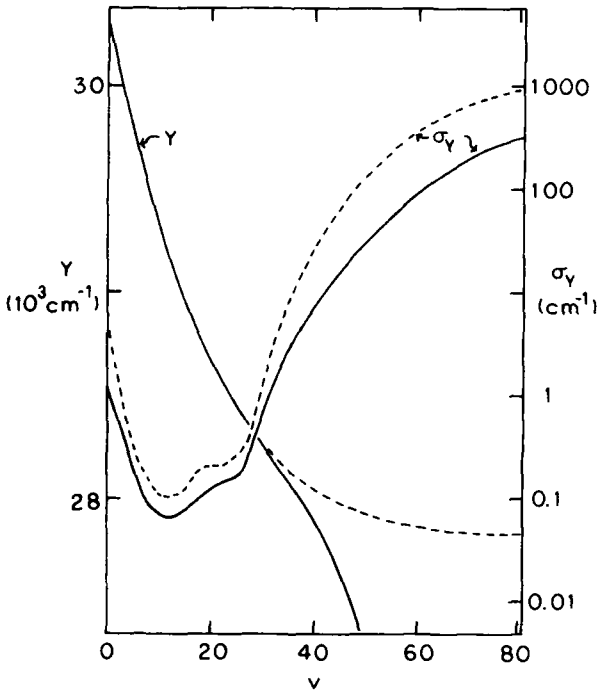

FIG. 2. Plots of $Y \equiv \Delta T_e - G_v$ and its error σ_Y as functions of v for the A' state of I_2. The solid curves represent results of the $P_{2,4}$ polynomial fit, dashed curves the $F_{a,3}$ near-dissociation fit. Note the logarithmic scale for σ_Y.

fits, since $\mathfrak{D}_e$ and v_D are so ill-determined in the seven- and eight-parameter fits. The result would be an apparently very precise value of 2372.6 cm^{-1} for $\mathfrak{D}_e$, which is ~ 130 cm^{-1} (or about $\frac{1}{4}$ the extrapolation energy) below the correct value. It is clearly necessary to more fully sample the model dependence. A way of doing so with the framework of the F_a and F_b forms is to drop various powers of $(v_D - v)$. This method is explored further in the Br_2 work discussed below.

One troubling feature associated with model dependence is the observation that *bad* fits having few parameters can often yield apparently more precise estimates than *good* fits having more parameters. For example the six-parameter fits in Table I all yield systematically high values of ΔT_e, with precision comparable to or better than that of the seven-, eight-, and nine-parameter fits. A second case of "model deception" is illustrated in Fig. 2, which shows the quantity $(\Delta T_e - G_v')$ and its error band for the $P_{2,4}$ and $F_{a,3}$ fits. The error for the latter is larger everywhere, even though the estimation of levels between the highest observed v'' level and v_D'' must surely be better for the NDE. To avoid such problems it may be wise to confine the model weighting to fits having form and quality comparable to that of the best fit.

In one other test calculation using the I_2 data, I investigated the effect of changing the C_5 value. For the $B(0_u^+\ ^3\Pi)$ state of I_2 the best experimental estimate[20] of C_5 is a factor of 1.56 smaller than the value given in Ref. 19. Reduction of the C_5 for the A' state by the same factor yields a value of 1.7×10^5 cm^{-1} Å^5, which increases X_n by 34% and the limiting slope in Fig. 1 by 13%. The NDE fits conducted with this X_n were comparable in quality to the previous fits, and the convergence problem persisted for more than six parameters. In keeping with expectations the estimates of $\mathfrak{D}_e$ changed by only 9 cm^{-1} for the $F_{a,2}$ fit and 29 cm^{-1} for the (very uncertain) $F_{a,3}$ fit.

B. Br_2 $(D' \rightarrow A')$

A detailed analysis of the $D' \rightarrow A'$ system in Br_2 has been published recently.[21] The final recommended constants for this system were obtained from a global fit of all assigned rotational lines and band heads for the (79, 79), (79, 81), and (81, 81) isotopic Br_2 molecules, and spanned v' levels 0–6 and v'' levels 5–21. The highest observed v'' levels appeared to follow the calculated limiting behavior in the plot equivalent to Fig. 1, and a linear extrapolation gave $\mathfrak{D}_e = 2835$ cm^{-1} and $v_D = 53.9$. To avoid the additional complications of including rotational structure and multiple isotopes, I have used in the present calculations just the red-degraded bandheads for $^{79}Br_2$ listed in Table I of Ref. 21. These bands sample the somewhat smaller v'' range, 5–16. For C_5 I have used the same value used in Ref. 21 $(1.39\times10^5$ cm^{-1} Å$^5)$.

These calculations showed behavior similar to that described for the I_2 data. Four vibrational parameters were again needed for an adequate representation of G_v'' in the polynomial fitting, and two sufficed for the upper state. Additional parameters gave no significant improvement. In the NDE fits, five parameters were clearly inadequate, and the fits containing more than six again failed to converge. The six-parameter fits gave variances only slightly higher than the benchmark $P_{2,4}$ fit.

Figure 3 illustrates the results of these calculations. The aforementioned problem of the incorrect slopes is even more evident here. Figure 4 shows that in the region very close to v_D the slopes approach the correct values, as indeed they must. However, it is clear that the behavior is deviating from the limiting behavior much too rapidly with increasing $(v_D - v)$, because the correction functions are "turning on" too quickly. To produce a more reasonable extrapolation, I experimented with higher lead powers of $(v_D - v)$ in F_a. The curves for $F_{a,2}$ (2, 4) [i.e., terms of powers 2 and 4 in $(v_D - v)$] in Figs. 3 and 4 show that dropping the linear term produces considerable improvement. The use of still higher powers gave even longer near-linear extrapolations, with the estimated $\mathfrak{D}_e$ value approaching ~ 2820 cm^{-1} for the highest powers investigated [$F_{a,2}(7, 8)$]. The variances of all of these six-parameter fits having no linear correction term were only marginally higher than that for the seven-parameter $P_{2,4}$ fit.

With the importance of choice of lead power so evident I returned to the five-parameter NDE fits [i.e., those having only one term in $(v_D - v)^j$ in the correction function]. Remarkably the variance decreased progressively as j was increased, until for $j = 7$ this five-parameter fit actually outperformed the seven-parameter polynomial fit! Further increase in j led to immediate

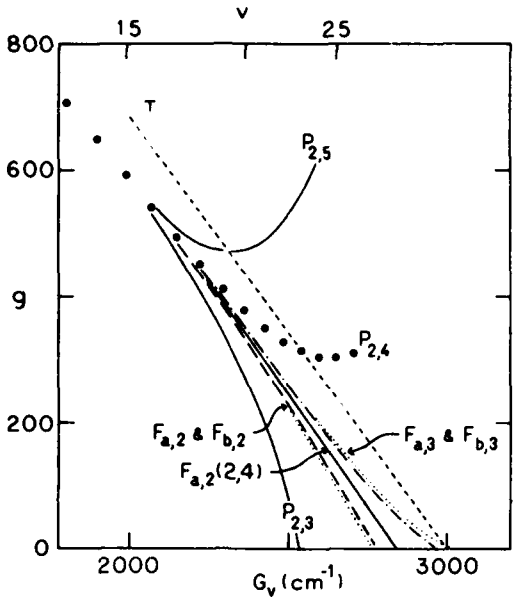

FIG. 3. g (cm$^{-10/7}$) vs G_v for the $A'(2u)$ state of Br_2. The dashed line (T) indicating the theoretical limiting behavior is arbitrarily drawn to intercept the G_v axis at 3000 cm^{-1}. Other curves are as identified in Fig. 1 and are adjusted to have coincident $G_v(15)$ values.

deterioration in the fit quality. As j was increased from one to nine, the estimate of $\mathfrak{D}_e$ decreased monotonically from 3091.6(6.8) to 2751.8(2.4) cm^{-1}; concomitantly, ΔT_e decreased from 35 747.6(4.3) to 35 594.6(3.5) cm^{-1}. (Because of the changing ΔT_e, the extrapolated energy from the highest observed level actually varies only half as much as does $\mathfrak{D}_e$.) In keeping with the previous comments about problems with model dependence, it is worth noting that the error estimate on the unreasonably large first $\mathfrak{D}_e$ value is a factor of 2 smaller than those on the more reasonable values from the six-parameter fits. The optimal five-parameter fit gave the following results: $\Delta T_e = 35\,645.9(1.8)$ cm^{-1}, $\mathfrak{D}_e = 2820(1.0)$ cm^{-1}, $v_D = 48.444(10)$, and $a_7 = -1.7821\times10^{-13}$. The ΔT_e value is 15–55 cm^{-1} smaller than the estimates from the polynomial fits, which in fact do not pin this quantity down very well.

As for the I_2 calculations, all NDE fits having variances within a factor of 2 of the minimum gave mutually consistent values for the upper state vibrational parameters. Weighted averages from these same fits yielded the following results: $\Delta T_e = 35\,654(5)$ cm^{-1}, $\mathfrak{D}_e = 2828(8)$ cm^{-1}, and $v_D = 48.42(7)$. Although these averages were obtained from results of 14 fits, they were dominated by the contributions from the three included five-parameter fits $F_{a,1}(6)$, $F_{a,1}(7)$, and $F_{a,1}(8)$. The $\mathfrak{D}_e$ and v_D values are reasonably close to those obtained from the full data set by graphical extrapolation.[21] Of course, their validity rests on the assumption that behavior such as that observed for $I_2(A')$ does not set in above the highest observed level. In view of that possibility for the lengthy extrapolation (~400 cm^{-1} from $v = 21$), the error estimates are probably optimistic.

C. XeCl ($B \rightarrow X$ and $D \rightarrow X$)

For these calculations I have used the bandhead measurements for $^{136}Xe\,^{35}Cl$ reported in Ref. 22. These data span $v = 0$–12 in the B state, 0–9 in D, and 0–13 in X. Here, $n = 6$, and I have used the C_6 value of 8×10^5 cm^{-1} Å^6 estimated in Ref. 6. The optimal polynomial fit of Ref. 22 contained ten parameters—T_e, ω_e, and $\omega_e x_e$ for each upper state, and four vibrational parameters for the X state. Graphical extrapolation yielded an estimated $\mathfrak{D}_e$ of 281(10) cm^{-1}.

In the NDE fits both transitions were fitted simultaneously, as they were in the polynomial fits. For the X state, correction functions containing only one term in $(v_D - v)^j$ were not adequate. However all two- and three-term functions (nine- and ten-parameter fits) gave convergence, with variances mostly within 10% of that for the polynomial fit. Since the data set included $v'' = 0$, there was very little spread (0.3 cm^{-1}) in the T_e estimates. As before, there was complete consistency in the various estimates of the B- and D-state vibrational constants. In this case the extrapolation from the highest observed level of the X state to $\mathfrak{D}_e$ is short, and the fits were only weakly sensitive to choice of powers of $(v_D - v)$ in the correction function. For example in the nine-parameter fits to $F_{a,2}$, $\mathfrak{D}_e$ decreased from 285.4(8) cm^{-1} to 277.4(6) cm^{-1} as the powers of $(v_D - v)$ were increased from (1, 2) to (3, 6). Weighted averages of results from 11 fits yielded $\mathfrak{D}_e = 281.1(7)$ cm^{-1}, $v_D = 19.30(10)$.

The original analysis of the XeCl B–X system[6] employed sources containing Xe and Cl in natural isotopic abundance. The spectra sampled the smaller v'' range 0–7 and yielded (by graphical extrapolation) a signifi-

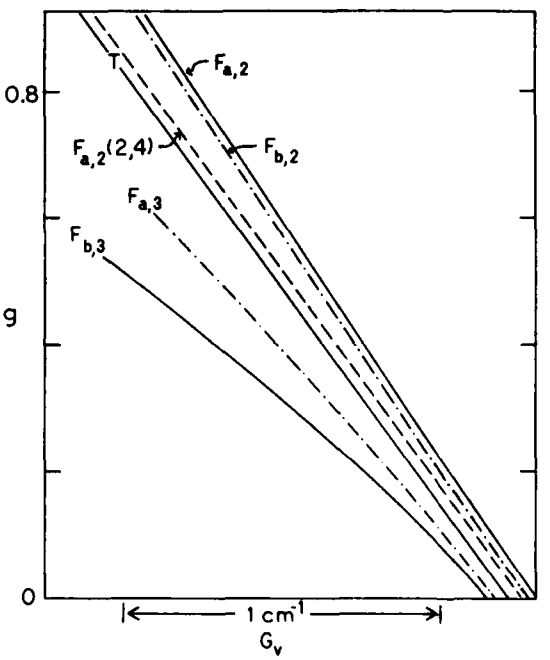

FIG. 4. Near-dissociation curves of Fig. 3 in the region very near the dissociation limit. The G_v scales have been adjusted to emphasize the comparisons.

cantly smaller estimate of $\mathfrak{D}_e = 255(10)$ cm^{-1}. On reprocessing these data with the present direct fitting method, I obtained 273(4) cm^{-1}, which is significantly closer to the current best estimate. For comparison a refit of the 1978 data, truncated to the same bands included in the 1975 analysis, yielded $\mathfrak{D}_e = 278(3)$ cm^{-1}, which is within one standard error of the value obtained from the full data set.

IV. SUMMARY

From these calculations, I draw the following conclusions:

(1) Near-dissociation expansions can represent vibrational energies with efficiency comparable to that of the customary polynomials in $(v+\frac{1}{2})$. This result bears out indications of previous studies[9,23–25] (in which, however, no explicit NDE-vs-polynomial comparisons were given). For data sets lacking data for low v levels, the extrapolations to $v=\frac{1}{2}$ show precision and model-dependent scatter comparable to those for polynomial fits. For extrapolation to large v, the NDE fits *must* perform better, as they are designed to approach dissociation correctly. Since these fits are nonlinear, convergence problems may occur, especially for higher fit dimensions.

(2) The near-dissociation fits may *not* yield very good long-range behavior, even though the NDEs are constrained to have the correct n and C_n values. Their performance can be improved by excluding low orders of $(v_D - v)$ from the correction functions. There is some theoretical justification for this step,[26] from consideration of higher-order contributions to the long-range potential. Although one could incorporate additional constraints in the NDE to reflect these higher-order contributions, such a move is hardly warranted in the present examples, where the vibrational levels sampled by the data are far from the dissociation limit. However, it is advisable to at least examine the NDEs graphically, to ensure that unacceptable behavior like that of some of the curves in Figs. 1 and 3 be avoided.

(3) There is no simple prescription for quantitative assessment of model dependence, as the range of possible correction functions is essentially unlimited. To avoid some of the problems of model error, it may be wise to consider in the final evaluation only fits having quality comparable to that of the "best" fit. In the present calculations, only the correction functions of Eqs. (7) and (8) have been examined. Rational polynomials[23–25] or exponentials[12] may prove better in many applications.

(4) In the cases investigated here, the vibrational constants for the upper states were consistent with the polynomial results, for all NDE fits having variances comparable to that of the best fit. This result suggests that one can, with negligible bias and correlation error, fit to a modified form of Eq. (9), in which G'_v is taken as known. However, one should *not* fit the polynomial-derived G''_v expression directly, as this quantity may already contain considerable model dependence. This point is particularly relevant for limited data sets, such as those for the D'–A' systems of I_2 and Br_2, where ΔT_e and G''_v are strongly dependent on polynomial order.

(5) The achievement of a good NDE fit for a limited data set should never be accepted as an excuse for not seeking additional data. The reason is that no fit can be expected to correctly account for behavior such as that of $I_2(A')$ in Fig. 1 unless the data sample the relevant regions. This type of behavior may be more the rule than the exception, since it occurs far from the asymptotic region where long-range theory should apply. In fact, work in my laboratory has shown similar effects for the A state of I_2[15,27] and the X states of the mercury halides[28,29]: In the former case the plot of Eq. (5) displays a slope which is about half the theoretical slope, until very close to the limit; in the latter the slopes exceed the limiting slopes for intermediate v, then approach the limit from above. In each case NDE fits to limited data sets would yield systematically erroneous $\mathfrak{D}_e$ values. In this light it may be provident to report errors in these determinations with an ounce of pessimism.

ACKNOWLEDGMENTS

I want to thank Robert LeRoy for suggestions following a critical reading of my original manuscript. This work was supported by the Office of Naval Research.

[1] R. T. Birge and H. Sponer, Phys. Rev. **28**, 259 (1926).
[2] G. Herzberg, *Spectra of Diatomic Molecules* (Van Nostrand, Princeton, 1950).
[3] R. J. LeRoy and R. B. Bernstein, Chem. Phys. Lett. **5**, 42 (1970).
[4] R. J. LeRoy and R. B. Bernstein, J. Chem. Phys. **52**, 3869 (1970).
[5] R. J. LeRoy, *Specialist Periodical Report on Electronic Spectroscopy*, edited by R. F. Barrow (Chemical Society, London, 1973), p. 113.
[6] J. Tellinghuisen, J. M. Hoffman, G. C. Tisone, and A. K. Hays, J. Chem. Phys. **64**, 2484 (1976).
[7] B. E. Wilcomb and R. B. Bernstein, J. Mol. Spectrosc. **62**, 442 (1976).
[8] R. J. LeRoy and W.-H. Lam, Chem. Phys. Lett. **71**, 544 (1980).
[9] D. L. Albritton, W. J. Harrop, A. L. Schmeltekopf, R. N. Zare, and E. L. Crow, J. Mol. Spectrosc. **46**, 67 (1973).
[10] D. L. Albritton, A. L. Schmeltekopf, and R. N. Zare, in *Molecular Spectroscopy: Modern Research*, edited by K. Narahari Rao (Academic, New York, 1976), Vol. II, p. 1.
[11] K. V. Subbaram, J. A. Coxon, and W. E. Jones, Can. J. Phys. **54**, 1535 (1976).
[12] J. W. Tromp and R. J. LeRoy, Can. J. Phys. **60**, 26 (1982).
[13] W. E. Deming, *Statistical Adjustment of Data* (Dover, New York, 1964).
[14] J. Tellinghuisen, M. R. McKeever, and A. Sur, J. Mol. Spectrosc. **82**, 225 (1980).
[15] J. Tellinghuisen, J. Mol. Spectrosc. **94**, 231 (1982).
[16] G. W. King, I. M. Littlewood, and J. R. Robins, Chem. Phys. **56**, 145 (1981).
[17] J. B. Koffend, A. M. Sibai, and R. Bacis, J. Phys. Paris (to be published).
[18] The work in Ref. 17 yields a precise determination of the A' state. However, from the nature of the data in the experiments of Refs. 15–17, it is likely that the extensive band head data of Ref. 15 provide the best determination of ω_e and $\omega_e x_e$ for the D' state. These values were used together with the

D' energy levels in Ref. 16 to estimate $T_{e,D'} = 40\,388.24(10)$ cm^{-1}. The ΔT_e value in Ref. 15 is in error due to lack of data for $v'' < 4$. For A' levels 6–22 the tabulated energies in Table III of Ref. 15 are 6.15–6.22 cm^{-1} below those in Table 7a of Ref. 17; therefore, the corrected ΔT_e value is 30 347.0 cm^{-1}. Accordingly, $T_{e,A'} = 10\,047.4$ cm^{-1}, and from the precisely known (Refs. 17 and 20) ground state dissociation energy ($\mathfrak{D}_{e,X} = 12\,547.20$ cm^{-1}), $\mathfrak{D}_{e,A'} = 2506.0$ cm^{-1}, with an estimated uncertainty of ~ 0.3 cm^{-1}.

[19]R. S. Mulliken, J. Chem. Phys. **55**, 288 (1971).

[20]G. W. King, I. M. Littlewood, J. R. Robins, and N. T. Wijeratne, Chem. Phys. **50**, 291 (1980).

[21]A. Sur and J. Tellinghuisen, J. Mol. Spectrosc. **88**, 323 (1981).

[22]A. Sur, A. K. Hui, and J. Tellinghuisen, J. Mol. Spectrosc. **74**, 465 (1979).

[23]A.-R. Hashemi-Attar, C. L. Beckel, W. N. Keepin, and S. A. Sorrleiter, J. Chem. Phys. **70**, 3881 (1979).

[24]A.-R. Hashemi-Attar and C. L. Beckel, J. Chem. Phys. **71**, 4596 (1979).

[25]C. L. Beckel and R. B. Kwong, J. Chem. Phys. **73**, 4698 (1980).

[26]R. J. LeRoy, J. Chem. Phys. **73**, 6003 (1980).

[27]K. S. Viswanathan, A. Sur, and J. Tellinghuisen, J. Mol. Spectrosc. **86**, 393 (1981).

[28]J. Tellinghuisen and J. G. Ashmore, Appl. Phys. Lett. **40**, 867 (1982).

[29]J. Tellinghuisen, P. C. Tellinghuisen, S. A. Davies, P. Berwanger, and K. S. Viswanathan, Appl. Phys. Lett. **41**, 789 (1982).

Appendix 4

MERCURY HALIDE SPECTROSCOPY

Joel Tellinghuisen
Vanderbilt University, Nashville, TN 37235

ABSTRACT

The B-X, C-X, and D-X transitions of HgCl, HgBr, and HgI are reanalyzed using Tesla discharge sources containing single isotopic species of these molecules. Direct, simultaneous least-squares fits of all transitions yield optimal vibrational constants for all four states. Low-resolution studies of the emission as a function of buffer gas pressure show effects of vibrational relaxation in the B state and collisional quenching of the C and D states. The broad B-A bands in the red and infrared are weak but clearly present, in support of a recent report of this transition in HgBr. In addition there is evidence of other transitions, previously unreported for these molecules, including a very weak system near 2200 Å in HgI, which shows fine red-degraded vibrational band structure.

INTRODUCTION

Although the mercury halide lasers are of considerable current interest, surprisingly little spectroscopic work has been done on the lasing $B(^2\Sigma^+) - X(^2\Sigma^+)$ transitions in the HgX molecules. The main source of information on these systems has been a series of papers published by Wieland over 20 years ago.[1-3] Most of Wieland's work involved sources containing the mercury halides in natural isotopic abundance. To refine the spectroscopic characterization of the HgX molecules, my group has been reanalyzing their emission spectra, using sources prepared from single isotopes of Hg and the halogens. Preliminary reports of our work on the B-X systems of HgCl, HgBr, and HgI have been published.[4,5] In this paper I discuss our continuing work on these systems and new work on the $C(^2\Pi_{1/2})$-X, $D(^2\Pi_{3/2})$-X, and B-$A(^2\Pi)$ systems. In addition we see evidence of weaker transitions, not previously reported.

HIGH-RESOLUTION STUDIES

Emission spectra have been photographed at high resolution from sources containing the individual isotopic species, $^{200}Hg^{35}Cl$, $^{200}Hg^{37}Cl$, $^{200}Hg^{79}Br$, $^{200}Hg^{81}Br$, $^{200}Hg^{127}I$, and $^{200}Hg^{129}I$, with excitation by means of a Tesla discharge.[6] Details of the preparation and operation of the sources have been given in the preliminary reports.[4,5] The sources show optimal emission in the visible B-X systems for HgX_2 pressures around 1 torr and Ar buffer

0094-243X/83/100099-07 $3.00

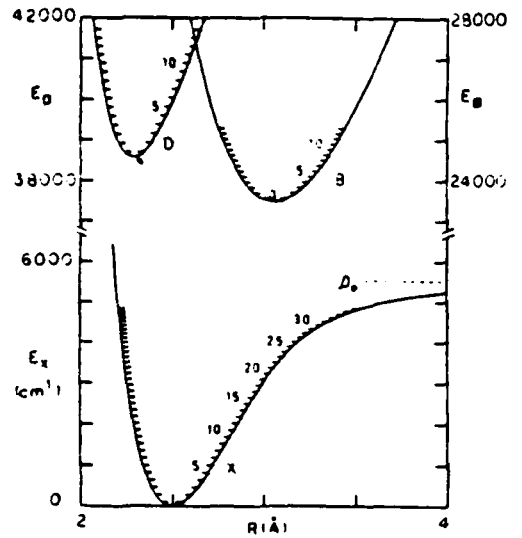

Fig. 1. Potential diagram for HgBr, showing levels of X, B, and D states spanned by the present emission analyses. Note different energy scales for all three states.

gas pressures around 200 torr. However, the C-X and D-X systems show evidence of quenching by Ar (see below), so Ar loading pressures <100 torr were employed in the sources used to record these systems.

While the B-X systems of these molecules show mainly red-degraded vibrational band structure, the C-X and D-X systems are mainly violet-degraded. The reason is that the C and D states lie at smaller internuclear distance than the X state, while the B state lies at considerably larger R. This situation is illustrated for HgBr in the potential diagram of Fig. 1, which shows the curves for the X, B, and D states. For the buffer gas pressures of our sources, considerable vibrational relaxation occurs in the excited states, so that the emission comes primarily from low v′ levels. Thus the B-X emission "samples" intermediate-to-high v levels of the X state, while the D-X and C-X systems sample the low-v′′ region. Although the B-X data span a much greater range of v′′ than do the C-X and D-X data, it is clear that the latter are needed for a proper description of the X states in the low-v region.

To date we have vibrationally analyzed the D-X systems in HgCl and HgBr, and have partially analyzed the C-X systems in HgBr and HgI. It appears that the rotational stucture in these systems is too congested to permit a rotational analysis, except possibly in the case of HgCl. However, we are able to position the D states relative to the X states through trial-and-error Franck-Condon calculations, as used for the B-X systems. Thus, for example, we find that the D state of HgBr lies about 0.07 Å to small R from the X state, as shown in Fig. 1. For the B-X systems our vibrational analyses have been completed for HgI[7] and are nearing completion for HgCl and HgBr. Our rotational analyses for the latter two molecules are still in progress. For HgI a rotational analysis has not been possible,

Table I. Vibrational constants (cm^{-1}) for X, B, and D states of ^{200}Hg ^{35}Cl.

	$X(^2\Sigma^+)$	$B(^2\Sigma^+)$	$D(^2\Pi_{3/2})$
T_e	0	23422.3	39703.4
c_{v1} (ω_e)	293.353	191.985	342.130
c_{v2} ($-\omega_e x_e$)	-1.7692	-0.5033	-1.8707
c_{v3}	-7.741×10^{-4}		
c_{v4}	-3.966×10^{-4}		
σ		0.51	
v range	0-31	0-25	0-13
no. of bands	126	79	47

because the B-X system is extremely congested. However, computer simulations of the unresolved rotational structure in the vibrational band contours indicate clearly that spin splitting is significant in these systems, meaning that a four-branch model is needed to account for the rotational structure, just as it is for the B-X system of XeF.[8]

To obtain optimal vibrational constants for these emission systems, we employ a direct, simultaneous least-squares fit of all transitions. Preliminary constants from these fits for the B-X and D-X transitions in HgCl and HgBr are given in Tables I and II. Although these constants are not final, I do not expect them to vary

Table II. Vibrational constants (cm^{-1}) for X, B, and D states of ^{200}Hg ^{79}Br.

	$X(^2\Sigma^+)$	$B(^2\Sigma^+)$	$D(^2\Pi_{3/2})$
T_e	0	23489.2	38572.9
c_{v1}(ω_e)	188.982	135.934	231.232
c_{v2} ($-\omega_e x_e$)	-1.0710	-0.2534	-0.9897
c_{v3}	-1.210×10^{-3}		
c_{v4}	-2.407×10^{-4}		
σ		0.36	
v range	0-30	0-13	0-14
no. of bands	164	92	72

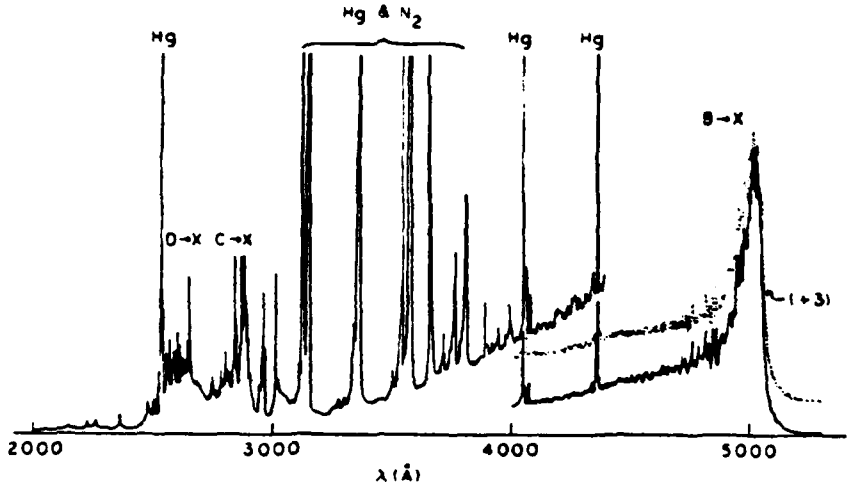

Fig. 2. Tesla discharge emission spectra of $^{200}Hg^{81}Br$ recorded at low resolution using a 0.3-m monochromator. The spectra were obtained from sources having Ar buffer gas loading pressures of 200 torr (solid curve) and 60 torr (dotted), illustrating effects of vibrational relaxation on the B-X emission. The spectra have not been corrected for the spectral response function of the spectrometer, which is approximately flat from 2800 to 3700 Å, but lower in sensitivity (in units proportional to quanta/Å) by a factor of 2 at 2000 Å and a factor of 3 at 5500 Å. Note the scale change near 4000 Å.

significantly from their present values, for the purpose of representing the levels of these states over the stated ranges of the vibrational quantum number. While these parameters are valid only for the stated isotopic species, they may be used with confidence to calculate spectral wavenumbers for other HgX isotopic species, through the standard isotopic relationships and isotopic ρ factors.[4,5] On comparing our new constants with those given by Huber and Herzberg,[9] I find that the T_e, ω_e, and $\omega_e x_e$ values are in surprisingly close agreement. However, it should be noted that for [illegible] on the A state, [illegible] deviate from the previous assignments, leading to a roughly 1% decrease in the estimated dissociation energies.

LOW-RESOLUTION STUDIES

The emission spectra of all three molecules have been examined at low resolution from 2000 to 8000 Å, and for HgI and HgBr the emission has been studied as a function of Ar buffer pressure up to 1 atm. The UV-visible spectra of all three molecules are qualitatively similar to that shown for HgBr in Fig. 2. The peak intensities of the C-X and D-X systems are typically a factor of 3-10 smaller than those for B-X, with higher relative intensities at low Ar pressure than at high, indicating probable collisional quenching by Ar. In addition the C-X and D-X systems are more compressed on the wavelength scale, so the total C-X and D-X emission is about a factor of 20-50 weaker than B-X. In HgBr and HgI, C-X and D-X are about equal in intensity; in HgCl D-X is considerably stronger than C-X.

To the red of the B-X systems we see evidence of at least two transitions, probably diffuse (bound-free). With increasing pressure

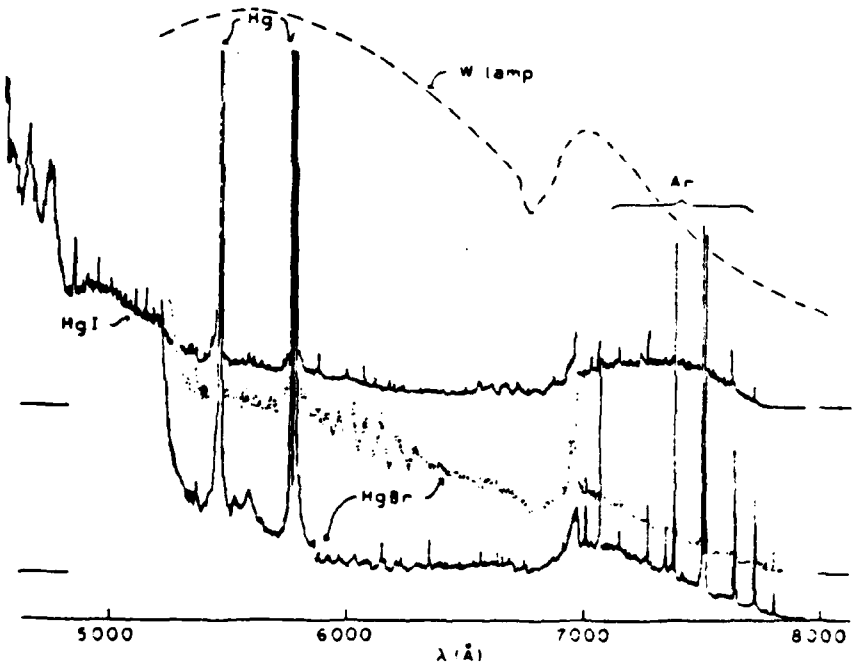

Fig. 3. Emission spectra of HgBr in Ar at 725 torr (solid) and 200 torr (dotted), and HgI in Ar at 710 torr. Also shown is the response to a quartz-halogen tungsten lamp (with zero of intensity the same as for the HgI spectrum).

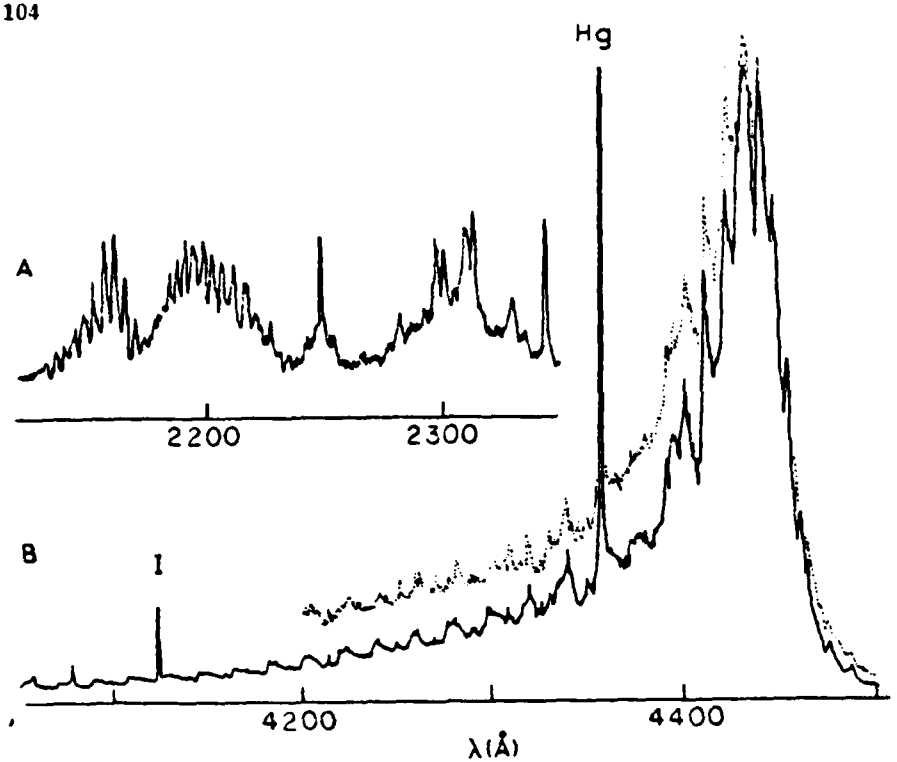

Fig. 4. HgI emission spectra. (A) Weak, red-degraded system in the ultraviolet. (B) B-X system at Ar pressures of 710 torr (solid) and 105 torr (dotted).

the total emission in this region for HgI and HgBr decreases relative to B-X, indicating a contribution from some excited state other than B (see Fig. 3). However, in some spectral regions the emission tracks the B-X system in intensity, indicating that it originates from the B state. In agreement with Lapatovich, et al.,[10] we attribute this emission to the B-A transition. In HgI there appear to be two such bands, probably the B-A(3/2) and B-A(1/2) components. In both molecules there is some structure superimposed on the continuum, which declines with increasing pressure. The latter effect is attributable to vibrational relaxation within the B state, which is clearly evident in the B-X system (see Fig. 4B).

In the ultraviolet we find evidence of one or more additional electronic transitions, an order of magnitude weaker than C-X and B-X, and previously unreported. In HgI a system near 2200 Å shows a fine red-degraded band structure (Fig. 4A). As we have just begun to look at these systems, we can venture no guess of their electronic assignment yet. Other projects still in an early stage of development in my laboratory include (a) an experimental determination of the B-X electronic transition strength function, and (b) measurements of collisional line broadening using Fabry-Perot interferometry.

This work was supported by the Office of Naval Research.

REFERENCES

1. K. Wieland, Helv. Phys. Acta 2, 46 (1929).
2. K. Wieland, Helv. Phys. Acta 14, 420 (1941).
3. K. Wieland, Z. Elektrochem. 64, 761 (1960).
4. J. Tellinghuisen and J. G. Ashmore, Appl. Phys. Lett. 40, 867 (1982).
5. J. Tellinghuisen, P. C. Tellinghuisen, S. A. Davies, P. Berwanger, and K. S. Viswanathan, Appl. Phys. Lett. 41, 789 (1982).
6. M. R. McKeever, A. Sur, A. K. Hui, and J. Tellinghuisen, Rev. Sci. Instrum. 50, 1136 (1979).
7. K. S. Viswanathan and J. Tellinghuisen, J. Mol. Spectrosc. (in press).
8. J. Tellinghuisen, P. C. Tellinghuisen, G. C. Tisone, J. M. Hoffman, and A. K. Hays, J. Chem. Phys. 68, 5177 (1978).
9. K. P. Huber and G. Herzberg, Constants of Diatomic Molecules (Van Nostrand Reinhold, New York, 1979).
10. W. P. Lapatovich, G. R. Gibbs, and J. M. Proud, Appl. Phys. Lett. 41, 786 (1982).

Note Added (August, 1983): The HgI spectra shown in the inset to Fig. 4 have been observed and studied previously. These transitions are identified in Ref. 9 as the H-X, G-X, and F_i-X (i = 1-3) systems. Our studies generally confirm the previous results for the first two but not for the F-X systems.

Appendix 5

JOURNAL OF MOLECULAR SPECTROSCOPY 98, 185–198 (1983)

The $B(^2\Sigma^+) \rightarrow X(^2\Sigma^+)$ Transition (4050–4500 Å) in HgI

K. S. VISWANATHAN AND JOEL TELLINGHUISEN

Department of Chemistry, Vanderbilt University, Nashville, Tennessee 37235

The $B \rightarrow X$ band system (4050–4500 Å) of HgI is photographed and vibrationally analyzed for the isotopically pure species $^{200}Hg^{127}I$ and $^{200}Hg^{129}I$. The assigned bands span v'' levels 5–26 and v' levels 0–13. The least-squares analysis indicates that the previously accepted v'' numbering for this system is one unit too high. Band-profile simulations and Franck–Condon calculations indicate that the internuclear separation (R_e'–R_e'') is 0.49 Å. The ground-state dissociation energy ($\mathcal{D}_e$) is estimated to be 2750 ± 80 cm^{-1}. Spin splitting is found to contribute significantly to the band structure.

INTRODUCTION

The $B \rightarrow X$ emission systems of the diatomic mercury halides (HgX) have become a subject of renewed interest in recent years, following the discovery of strong lasing on these transitions (*1–3*). The most recent comprehensive studies of these bands were reported by Wieland (*4–6*) over 20 years ago. Wieland's HgBr and HgI sources contained HgX_2 in the natural isotopic mixture. In the case of HgCl he used isotopically enriched Cl_2, but still natural Hg. To refine the spectroscopic characterization of these systems, we have undertaken a study of the $B \rightarrow X$ transitions, using isotopically pure mercury and halogen in our sources. Such single-isotope sources have been used to great advantage in previous works from this laboratory (*7–9*).

We have recently reported preliminary results of our work on HgBr (*10*), and HgCl and HgI (*11*). In this paper we present our detailed analysis of the $B \rightarrow X$ transition in HgI—the band with peak intensity near 4450 Å. Our interpretation of the spectrum agrees qualitatively with Wieland's work (*6*), except at the long wavelength end. However, our least-squares analysis indicates that the v'' numbering suggested by Wieland is one unit too high. Our computational analysis includes band-profile simulations and Franck–Condon calculations to corroborate the assignments of many of the features in the spectrum and to deduce the relative configuration of the B and X potential curves.

EXPERIMENTAL SECTION

In recording the spectra, we used procedures similar to those described previously (*7–9*). The sources consisted of 3-mm o.d. pyrex tubes about 10 cm long, which were charged initially with $^{200}Hg^{127}I_2$ (or $^{200}Hg^{129}I_2$) and ~200 Torr Ar, then sealed off with a torch. The ^{200}Hg (95.7% isotopic purity, Oak Ridge) was obtained in the form

0022-2852/83 $3.00

of HgO, which was decomposed *in situ* by heating under vacuum. Iodine vapor was then admitted in excess, and the mixture was gently heated to yield HgI_2.

The $^{129}I_2$ used to make the $^{200}Hg^{129}I$ sources had previously been prepared from a basic $Na^{129}I/Na_2SO_3$ solution (Oak Ridge, ~99% isotopic purity) by acidifying with HNO_3 and oxidizing with $NaNO_2$, with the operations carried out in an ice bath to reduce sublimation losses. The $^{129}I_2$ was collected by centrifugation. Excess water was removed by trap-to-trap distillation in the presence of dry P_2O_5.

The emission was excited with a Tesla coil (*12*), with the source mounted in a ceramic holder heated to ~160°C to maintain a suitable vapor pressure (~1 Torr) of HgI_2. The spectra were photographed on Kodak 103a-F plates in the first order of a JY HR 1500 1.5-m spectrometer equipped with a 3600-groove/mm holographic grating. The emission was recorded for the region 4050–4500 Å, with a reciprocal dispersion of about 1.1 Å/mm. For typical slit widths of 10–50 μm, exposures ranged about 2–12 min. Slit widths of 100 μm were used in the shorter wavelength region, where the emission was weaker. This system was also photographed at lower resolution (reciprocal dispersion ~5.0 Å/mm) using a 1200-groove/mm grating. Iron calibration spectra were obtained from a microwave discharge Fe/I_2 lamp using exposures of ~5 sec. The plates were developed 4 min in Kodak D-19 developer. The spectra were measured on a Grant comparator. The Fe calibration lines were fitted to low-order polynomials with typical standard deviations of 0.002–0.003 Å. Most of the measured features in the high-resolution spectra were estimated to be precise to about 0.2–0.3 cm^{-1}.

RESULTS AND DISCUSSION

Assignments

Figure 1 displays the emission spectra for both isotopic species in the region 4410 to 4490 Å. Qualitatively, this spectrum resembles the 2770-Å system in I_2 (*8*) and the 3100-Å system in Br_2 (*13*). At its long wavelength end it displays many violet-degraded and spikelike features. However, towards shorter wavelengths the spectrum is dominated by red-degraded heads, indicating that the upper state potential curve is shifted to larger internuclear distance relative to the lower state potential. Consequently the emission from low v' levels terminates on the attractive branch of the lower state. This pattern is typical for transitions from ion-pair excited states.

At the outset we sought an assignment scheme in terms of a vibrationally relaxed emitting state, with dominant emission from low v' levels. This model of a nearly thermalized emitting state has proven correct for other halogen and rare-gas halide emissions from Tesla discharge sources at moderate buffer-gas pressures (*7–9*). Initially we concentrated on the red-degraded features. For these the errors resulting from the measurements of the bandheads rather than the origins are insignificant, since the head-to-origin (H–O) corrections are generally 0.2 cm^{-1} or less. For the violet-degraded and spikelike features, we used band-profile simulations to arrive at the H–O shifts. All of these features are included in our final least-squares fit. We have made no attempt to analyze rotational structure, because the spectrum is rotationally very congested. However, we have been able to deduce information on the rotational constants from band-profile and Franck–Condon calculations.

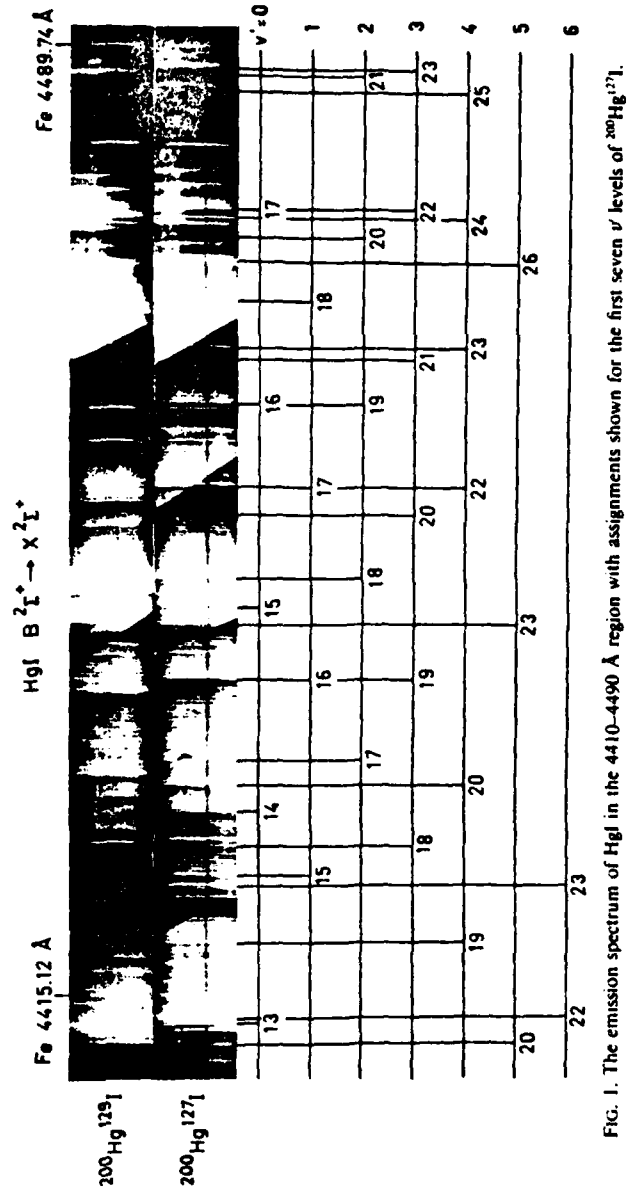

FIG. 1. The emission spectrum of HgI in the 4410–4490 Å region with assignments shown for the first seven v' levels of $^{200}Hg^{127}I$.

TABLE I

Estimated Band Origins of Assigned Bands of $B - X$ System of ^{200}HgI[a]

v'-v''	Weight	($^{200}Hg^{127}I$)	Δv[b]	Weight[c]	($^{200}Hg^{129}I$)	Δv
3-23	3	22273.6	-0.2		22277.4	0.1
2-21	7	276.9	-0.1		281.7	0.0
4-25	3	284.0	-0.1		287.0	0.2
(3-22)[d]		328.9				
4-24	3	331.7	0.0			
5-26	3	348.6	0.0		351.0	0.2
1-18	10	364.5	0.1		370.2	-0.1
3-21	7	386.7	0.0			
0-16	10	404.9	-0.1		410.9	-0.2
2-19	10	404.9	0.1		409.7	0.3
1-17	10	438.2	-0.1		443.5	0.1
4-22	7	437.8	-0.1		441.3	0.1
2-18	10	474.9	-0.2	1	480.4	-0.7
0-15	1	485.9	-0.3	10	491.5	-0.1
5-23	3	492.6	-0.5		495.2	0.0
1-16	10	515.2	0.1	1	520.3	0.4
(3-19)		515.4				
2-17	10	548.2	0.0		553.6	-0.4
4-20	10	558.2	0.2		562.5	-0.2
0-14	10	569.8	0.2		575.7	0.0
1-15				1	602.2	-0.8
5-21				7	608.8	-0.1
4-19	1	623.9	0.4	10	628.1	0.2
6-22	7	655.6	0.2			
7-24	3	658.7	-0.4			
0-13				10	663.3	0.0
5-20	10	667.3	0.2		670.7	0.3
2-15				1	711.8	-0.8
8-25	3	718.6	0.1			
3-16	10	735.0	0.3			
0-12	10	749.1	-0.1		754.3	-0.0
7-22	7	764.5	-0.2			
1-13				10	773.0	0.3
2-14	10	790.7	-0.1		795.5	-0.2
8-23	3	817.5	0.2		819.2	0.1
0-11	10	843.4	0.0		848.3	0.1
1-12	10	859.4	0.1		864.1	0.1
0-10	10	940.9	0.1			
1-11	10	953.8	0.1		958.2	0.2
9-22	7	980.8	-0.4		981.2	0.4
3-13	1	988.6	-0.3	10	992.5	-0.3
10-23	3	23032.9	0.2	1	23034.0	-0.3
1-10				10	055.5	0.1
6-16	10	062.8	0.0			
2-11	10	064.0	0.1		067.8	0.2
(10-22)					088.6	
11-23	3	140.9	-0.5		140.2	0.3
2-10	1	161.5	0.2		165.3	-0.1
2-9	10	262.3	-0.2	1	265.8	-0.4
3-10	1	271.2	0.2		274.5	0.0

The estimated band origins of all bands included in our final least-squares fit are given in Table I. For bands involving $v'' < 21$, the H–O corrections are nominal (0.2 cm^{-1} or less). For bands involving higher v'', the H–O shifts were calculated for each feature, as in these cases the corrections are large and more sensitive to the individual B_v values. Our measurements of most of the red-degraded bands agree with those of Wieland within 1 cm^{-1}; however, our values tend to be slightly lower than his. This systematic shift is consistent with the isotope shift for our $^{200}Hg^{127}I$ spectra vs the $^{200}Hg^{129}I$ which should have predominated in Wieland's sources. With the previously mentioned change in the v'' numbering, our assignments generally agree with Wieland's for bands having $v'' < 18$ (our numbering). For larger v'' our assignments deviate

TABLE I—*Continued*

v'-v''	Weight	($^{200}Hg^{127}I$)	Δv	Weight	($^{200}Hg^{129}I$)	Δv
13-23	3	354.1	-0.2			
3-9	1	371.8	0.1	10	374.5	0.2
3-8	10	475.1	0.2		477.7	0.0
4-9	10	481.5	-0.1		484.0	-0.3
4-8	10	584.8	0.0		587.0	-0.3
5-9				10	592.1	0.1
5-8	1	694.4	-0.4	10	695.3	0.0
5-7	10	800.1	0.0	1	801.4	-0.3
6-8	10	803.2	-0.4		803.3	0.4
6-7				10	909.1	0.3
7-8				10	911.7	0.0
7-7	1	24017.5	0.0	10	24017.8	-0.4
8-7				10	125.1	0.0
9-7				10	232.3	0.2
8-6	10	234.6	-0.1	1	233.6	-0.1
(11-9)					237.0	
9-6	1	342.4	-0.1			
10-6	1	449.2	0.7		447.9	0.0
12-5	1	774.8	0.6			

[a] For bands involving $v'' \leq 10$ the origins were calculated to lie 0.1 cm^{-1} to the red of the measured feature; for $v''=11$-20 the corrections were 0.2 cm^{-1} in the same direction; for bands involving higher v'' the corrections were calculated for each individual feature.

[b] $\nu_{calc} - \nu_{obs}$ from least-squares fit.

[c] Weights for the 129 isotope have been mentioned only when different from those used for the corresponding 127 feature.

[d] Assignments in parentheses have not been included in the least-squares fit. Figures quoted for these assignments represent the measured features, not the estimated origins.

progressively to the blue of Wieland's, with the discrepancy amounting to ~40 cm^{-1} for the highest v'' level ($v'' = 25$) assigned by Wieland.

Band Structure

As in previous work, we used trial-and-error Franck–Condon calculations to account for the observed intensity pattern and to locate the upper state on the internuclear axis. For this purpose we employed a Morse potential for the excited state and a Morse–RKR (*10*, *14*) representation for the lower state, and we calculated FCFs (Franck–Condon factors) as a function of R_e'. We found that $\Delta R_e = 0.49 \pm 0.01$ Å best explained the observed intensity pattern. If we adopt Cheung and Cool's (*15*) estimate of 2.81 Å for the internuclear distance of the lower state, then R_e' is ~3.30 Å. This value is 0.03 Å greater than estimated by Cheung and Cool. Much of the difference can be attributed to a shift in the attractive branch of our X curve relative to theirs in the Franck–Condon region of strong emission. However, the FCF pattern is also different, as is discussed further below.

Since the upper state is shifted to larger internuclear distance relative to the lower state, most of the strong bands involving low v' are red degraded. With increasing v' the intensity maximum shifts to larger v'', and the individual bands begin to display violet-degraded edges to the red of the origin. Finally, with sufficiently large v'' the

bands are entirely violet degraded. This transformation arises because of the combination of (1) the rapid decrease of the lower-state rotational constant B_v with increasing v, (2) strong centrifugal distortion in the lower state, and (3) B_v values which decrease very slowly with increasing v'.

To understand the role of rotational structure in the band shapes, we carried out computer simulations of the band profiles, using procedures similar to those described previously (*8*, *13*, *16*). We first assumed a simple *P*- and *R*-branch structure. However, with this assumption we could not account for a large number of observed features or adequately explain the structures of several assigned bands (especially 7–24 and 4–24). We therefore introduced spin-splitting in the band structure. We adopted case b coupling for both states and assumed that all the splitting occurs in the lower state. This procedure is justified since the band profiles are sensitive only to the difference in the splitting. For selected v'–v'' bands we then calculated the rotational line frequencies using the relationship (*16*, *17*)

$$F_{e,f}(N) = B\kappa_{e,f} - D(\kappa_{e,f})^2 + H(\kappa_{e,f})^3 \qquad (1)$$

to represent the rotational energy, where

$$\kappa_e = N(N+1) + \alpha N; \qquad \kappa_f = N(N+1) - \alpha(N+1). \qquad (2)$$

The main effect of spin-splitting in the band structure is to split the extra features formed to the red of the origin, with the magnitude of the splitting being dependent on the splitting constant α. This is illustrated in Fig. 2, where the band profiles for the 3–22 band are plotted as a function of α''. By carrying out similar calculations for the 3–21 and 3–23 bands, we found that the value $|\alpha''| = 0.8$ best accounted for the observed structure in these bands. We then simulated profiles for bands involving higher v' and v'' levels. This procedure permitted us to assign almost every violet-degraded feature in our spectrum. Figures 3 and 4 illustrate the dependence of the band profiles on v'' for $v' = 7$. Even in the cases of the 7–24 and 4–24 bands, where the band shapes did not initially match, we find that with the introduction of spin-splitting there is reasonable agreement in shape.

Least-Squares Analysis

In our initial least-squares fits we included only those red-degraded bandheads for which the H–O correction is small compared with the precision of our measurements. On simultaneously fitting the assigned bands for both $^{200}Hg^{127}I$ and $^{200}Hg^{129}I$ to double polynomials in $(v' + 1/2)$ and $(v'' + 1/2)$, we obtained minimum variance for a v'' numbering one less than that suggested by Wieland. For Wieland's numbering the variance was almost a factor of two higher.

Once the v'' numbering was fixed, we expanded the fits to include the spikelike and violet-degraded features. These features are usually well removed from the origin (>2 cm^{-1}). The H–O corrections in these cases were determined from the band-profile calculations, using our best estimates of the rotational and spin-splitting constants. Because of uncertainties in the latter, the H–O corrections remain uncertain; consequently the estimated origins for these bands were given reduced weights in our

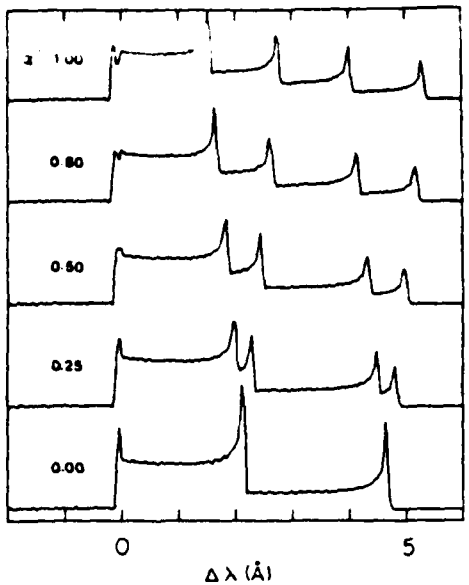

FIG. 2. Computer-synthesized band profiles for the 3–22 band, showing dependence on the splitting parameter α''. In these calculations a temperature of 450° K was assumed, and the resolution was taken as 0.05 Å. The upper-state constants were $B' = 0.01975$ and $D' = 2.58 \times 10^{-7}$. For the X state the rotational and distortion constants given in Table III were employed. The absolute wavelength and intensity scales are arbitrary, but a constant relative intensity scale is used for the five profiles in the figure. The origin of the wavelength scale is the band origin.

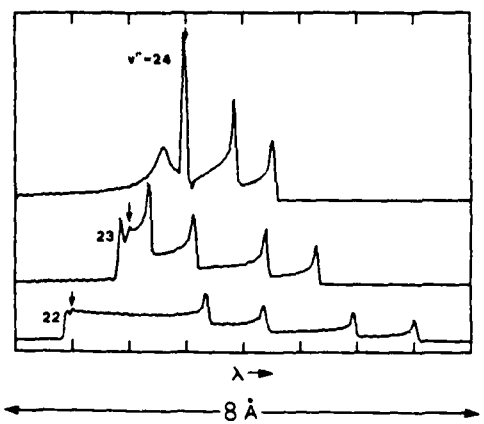

FIG. 3. Synthetic band profiles for selected bands involving $v' = 7$, calculated as in Fig. 2. The band origins are marked with arrows. A constant relative intensity scale is used throughout Figs. 3 and 4.

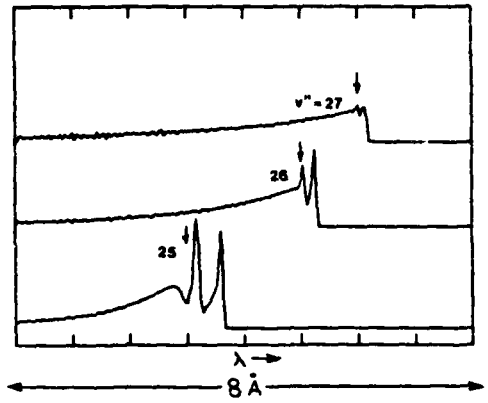

FIG. 4. Synthetic band profiles for $v' = 7$.

final fit. The assigned weights were 10, 7, and 3 for bands involving $v'' = 5$–20, 21–22, and 23–26, respectively; assignments from the low-resolution spectra were given weight 1. Minimum variance was obtained for an 8-parameter fit, containing 2 vibrational parameters for the excited state and 5 for the X state. Results are summarized in Table II, together with the rotational parameters obtained from a least-squares fit of the B_v values calculated as described below. These parameters represent the assigned bands with a standard deviation of 0.21 cm^{-1} and are valid for v' levels 0 to 13 and v'' levels 5 to 26.

Dissociation Energy

We have estimated the dissociation energy of the X state using long-range theory in a manner described by Wilcomb and Bernstein (*18*) and Tellinghuisen *et al.* (*19*). We employed the relation

$$g(G_v) \equiv \left(\frac{dG_v}{dv}\right)^{2n/n+2} = K_n^{2n/n+2}(\mathcal{D}_e - G_v) \qquad (3)$$

where $n = 6$. In our preliminary paper (*11*), we reported that the slope in the long-range plot for our then highest assigned level ($v'' = 23$) was greater than the theoretical limiting slope of −0.54 (*18*). This rendered the extrapolation to dissociation unreliable, and we were able to place only a rough upper limit on $\mathcal{D}_e$. Since we have now extended our assignments to $v'' = 26$, we are able to give a more precise estimate. In Fig. 5 we show the plots of (3) calculated from the least-squares parameters obtained in the fits of the assigned bands to representations containing 4-, 5-, and 6-term polynomials for G_v''. (All of these fits yielded comparable variances.) It is evident from these curves that the model dependence in the choice of polynomial order for the X state is the major source of uncertainty. For the 5- and 6-term representations the slope approaches the theoretical limiting value near $v = 27$; linear extrapolation yields $\mathcal{D}_e = 2800$–2830 cm^{-1} and $v_D \simeq 62$. For the 4-term polynomial, the curve intercepts the G_v axis at 2670 cm^{-1} without attaining the theoretical limiting slope. From these

TABLE II

Spectroscopic Parameters (cm^{-1}) for X and B State of $^{200}Hg^{127}I$[a]

	X ($^2\Sigma^+$)	B ($^2\Sigma^+$)
T_e	0.00	24071.99(452)
$c_{v1}(\omega_e)$	126.071 (1.3%)	110.810 (32)
$c_{v2}(-\omega_e x_e)$	−1.2704 (18%)	−0.1628 (27)
c_{v3}	1.5899×10^{-2} (98%)	
c_{v4}	-1.5785×10^{-3} (31%)	
c_{v5}	2.7681×10^{-5} (22%)	
σ	0.21	
$\mathcal{D}_e$	2750 (80)	38160 (80)[b]
c_{r1}	2.7470×10^{-2}	$1.9921\ (11) \times 10^{-2}$
c_{r2}	-1.8024×10^{-4}	$-2.83\ (21) \times 10^{-5}$
c_{r3}	-4.4990×10^{-6}	
c_{r4}	3.3617×10^{-7}	
c_{r5}	-2.5925×10^{-8}	
c_{r6}	4.7600×10^{-10}	
R_e (Å)	2.81[d]	3.302

[a] Vibrational constants are valid for v'=0-13, v''=5-26. Rotational constants are based on assumptions about potential curves; see text. Figures in parentheses are least-squares standard errors in last digits.

[b] Assuming dissociation to $Hg^+(^2S) + I^-(^1S)$. The lowest $Hg^+ + I$ asymptote lies 21,830 cm^{-1} lower.

[c] X-state rotational parameters are obtained from a least-squares fit of the caclculated B_v values in Table III.

[d] Assumed

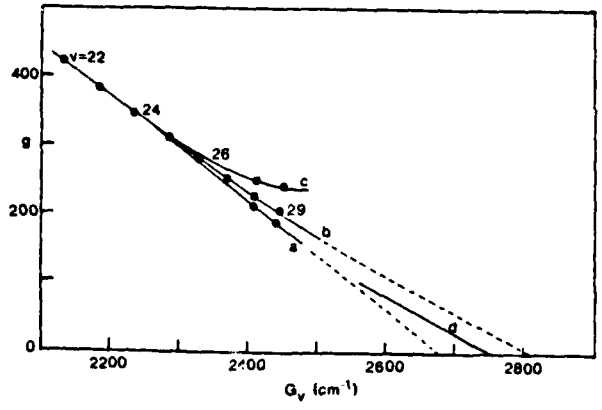

FIG. 5. Plot of g vs G_v and long-range extrapolations (--) for the X state, calculated from least-squares parameters obtained from (a) 4-, (b) 5-, and (c) 6-term polynomial representations for G_v. The solid line (d) represents the theoretical limiting slope of −0.54 (Ref. *18*).

results we consider that the ground-state dissociation energy is likely within 80 cm^{-1} of the value $\mathcal{D}_e'' = 2750\ cm^{-1}$. This value is about 300 cm^{-1} less than the estimate in (*18*), after correcting the latter value for the change in the v numbering.

Potential Curves and Derived Properties

For the purpose of the Franck–Condon and band-profile calculations, the X-state potential was approximated as a Morse–RKR curve (*14*), i.e., a Morse repulsive branch and an attractive branch obtained by adding to the repulsive branch the RKR turning point differences, $R_+(v) - R_-(v)$ (which are determined by the vibrational constants alone). For want of data below $v'' = 5$, $\omega_e x_e$ and (to a lesser extent) ω_e for the X state are poorly determined by our analysis. Consequently, to define the Morse repulsive branch we used the assumed R_e value of 2.81 Å, together with the experimental ω_e and a $\mathcal{D}_e$ value 40% greater than experiment (*14*). The resulting X-state potential and its computed spectroscopic constants are given in Table III. The D_v'' and H_v'' values were calculated using the energy derivative method (*20*). The potentials for both states are illustrated in Fig. 6. Note that the R_e values for both states are based on the assumption $R_e'' = 2.81$ Å (*15*), and hence remain experimentally unknown.

Estimates of the rotational constants for the B state were derived from the Franck–Condon and band-profile calculations, for the assumed X-state location and shape indicated above. The band-profile calculations were particularly useful in this regard, and yielded precise estimates for B_v for $v' = 3$, 4, 5, and 7. A least-squares fit of these values gave the B_e and α_e values in Table II. The α_e value is about 30% less than the value calculated for a Morse curve defined by the ω_e, $\omega_e x_e$, and B_e values. The difference appears to be statistically significant but is based on only the four values mentioned above.

TABLE III

Spectroscopic Constants (cm^{-1}) and Potential for the $X(^2\Sigma^+)$ State of $^{200}Hg^{127}I$[a]

v	T_v	$B_v \times 100$	$D_v \times 10^8$	$-H_v \times 10^{14}$	R_{min} (Å)	R_{max} (Å)
0	62.72	2.7376	0.53	0.4	2.7564	2.8743
1	186.29	2.7184	0.55	0.2	2.7202	2.9261
2	307.42	2.6987	0.57	0.5	2.6972	2.9652
3	426.14	2.6787	0.59	0.6	2.6796	2.9994
4	542.44	2.6582	0.61	0.7	2.6651	3.0309
5	656.30	2.6373	0.63	0.6	2.6527	3.0607
6	767.65	2.6157	0.66	0.8	2.6419	3.0895
7	876.43	2.5935	0.69	0.8	2.6323	3.1177
8	982.56	2.5705	0.73	1.0	2.6236	3.1456
9	1085.92	2.5465	0.77	1.0	2.6158	3.1735
10	1186.42	2.5215	0.81	1.4	2.6086	3.2016
11	1283.93	2.4954	0.87	1.6	2.6020	3.2301
12	1378.33	2.4680	0.93	1.9	2.5960	3.2592
13	1469.50	2.4392	1.00	2.2	2.5904	3.2891
14	1557.33	2.4089	1.08	2.6	2.5853	3.3199
15	1641.71	2.3771	1.17	3.1	2.5805	3.3518
16	1722.53	2.3436	1.27	3.6	2.5761	3.3851
17	1799.72	2.3084	1.38	4.3	2.5720	3.4198
18	1873.20	2.2715	1.51	5.3	2.5683	3.4562
19	1942.93	2.2328	1.65	6.2	2.5648	3.4946
20	2008.88	2.1924	1.80	7.2	2.5616	3.5350
21	2071.05	2.1503	1.96	8.4	2.5586	3.5776
22	2129.48	2.1066	2.14	9.8	2.5559	3.6227
23	2184.24	2.0610	2.33	11.1	2.5534	3.6703
24	2235.41	2.0155	2.52	12.5	2.5511	3.7207
25	2283.16	1.9687	2.70	13.6	2.5490	3.7737
26	2327.66	1.9218	2.86	13.9	2.5470	3.8293
27	2369.14	1.8754	2.99	12.8	2.5453	3.8872
28	2407.90	1.8305	3.05	10.4	2.5436	3.9468
29	2444.27	1.7881	3.04	9.9	2.5421	4.0076
30	2478.64	1.7481	3.09	21.0	2.5407	4.0678

[a] Since the vibrational analysis spanned v'' levels 5–26, the calculated constants outside this region are not reliable.

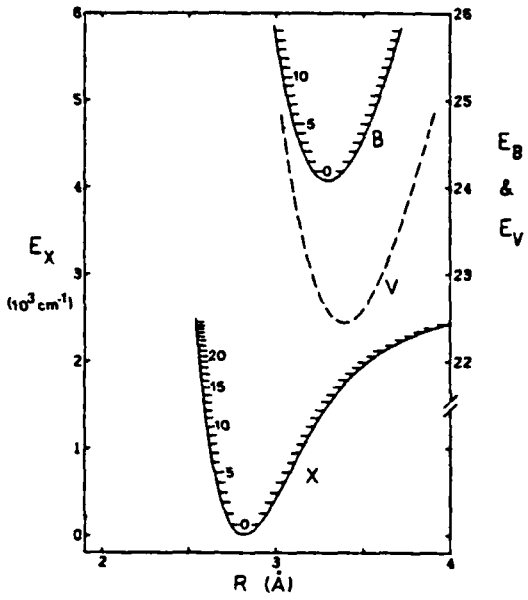

FIG. 6. Potential curves for the X and B states, and the difference potential (V). Note the different ordinate scales.

The Franck–Condon factors calculated for this system are listed in Table IV, for $J' = J'' = 0$ and $J' = J'' = 100$. The J dependence of the FCF is particularly important for the violet-degraded and spikelike features. However, the $J = 0$ values are appropriate for the red-degraded features, which occur at small J. The pattern of FCFs in Table IV is typical for an ion-pair $\rightarrow$ valence transition with a minimum in the difference potential near $R = R_e'$ (*9*).

Our FCF distribution is shifted up by about one v'' level from that of Cheung and Cool, after allowance for the change in v'' numbering for the latter. For example, the Franck–Condon gap for $v' = 1$ occurs near $v'' = 14$ in both calculations (corrected $v'' = 13$ in (*15*)). In keeping with the differences in the shape of the X curve, our distributions for low v' are also more sharply peaked. For example, our maximum FCF for $v' = 0$ is about 20% greater than the corresponding value in Table 12 of (*15*).

The FCFs in Table IV were calculated using a Morse B curve derived from the experimental ω_e, $\omega_e x_e$, and R_e values. We also calculated the FCFs employing an

TABLE IV

Franck–Condon Factors ($\times 10^3$) for $B \rightarrow X$ System in $^{200}Hg^{127}I$[a]

v''	v'=0	1	2	3	4	5	6	7	8	9	10	11	12	13
0	0	0	0	0	0	0	0	0	0	0	0	0	0	0
	0	0	0	0	0	0	0	0	0	0	0	0	0	0
1	0	0	0	0	0	0	0	0	0	0	0	0	0	0
	0	0	0	0	0	0	0	0	0	0	0	0	0	0
2	0	0	0	0	0	0	0	0	0	0	0	1	1	2
	0	0	0	0	0	0	0	0	0	0	0	1	1	2
3	0	0	0	0	0	0	0	0	1	1	3	5	7	11
	0	0	0	0	0	0	0	0	1	2	3	6	9	12
4	0	0	0	0	0	0	1	2	5	8	13	18	25	31
	0	0	0	0	0	1	2	3	6	10	15	21	28	34
5	0	0	0	0	1	3	6	11	18	26	35	41	45	45
	0	0	0	1	2	4	8	14	22	30	38	44	47	45
6	0	0	1	3	6	13	22	33	43	50	51	45	35	22
	0	0	1	4	8	16	27	38	47	52	50	42	29	16
7	0	1	4	11	23	37	50	57	55	44	28	12	2	0
	0	2	6	15	28	43	55	59	53	38	21	7	0	2
8	1	6	17	34	53	64	62	46	24	7	0	5	16	25
	1	8	22	42	60	67	59	38	16	2	1	10	22	28
9	5	21	46	69	74	57	28	6	0	10	24	31	25	13
	7	28	57	77	73	48	18	1	4	18	30	30	19	7
10	18	56	86	81	47	11	0	13	30	33	21	6	0	6
	26	70	94	76	33	3	4	23	35	30	13	1	2	12
11	54	106	93	37	2	10	33	38	21	3	2	13	23	21
	73	118	83	21	0	21	40	33	11	0	7	21	24	16
12	124	124	37	0	27	47	28	4	3	19	27	18	4	0
	156	114	17	7	42	44	15	0	12	27	24	9	0	4
13	213	63	1	46	50	12	2	22	31	16	1	4	16	21
	245	33	14	61	36	2	11	31	26	6	1	12	21	17
14	261	0	64	51	2	17	37	20	1	8	22	20	6	0
	262	13	82	28	2	33	34	7	2	19	24	11	0	4
15	211	96	63	0	38	37	4	8	27	20	3	3	15	19
	172	176	27	12	52	19	1	22	27	8	0	12	20	13

RKR B curve, generated using the rotational constants in Table II. The FCFs for strong bands changed by less than 10%, which is felt to be within the precision of our trial-and-error FCF and band-profile determination of the B-state rotational parameters. Consequently we have simply tabulated the Morse results.

CONCLUSION

In this work we have vibrationally analyzed the $B \rightarrow X$ system in HgI using single-isotope sources. The [illegible] analysis indicates that the v'' numbering suggested by Wieland is one unit too high. Due to the congested nature of the spectra, a rotational analysis was not possible. However, we extracted some information about the rotational structure of the bands using band-profile and FCF calculations to deduce the relative configuration of the upper and lower potential curves.

TABLE IV—*Continued*

v''	v'=0	1	2	3	4	5	6	7	8	9	10	11	12	13
16	96	262	2	55	29	2	29	26	3	6	21	18	3	1
	54	285	51	53	6	19	35	11	1	18	21	7	0	9
17	16	215	193	11	11	47	8	5	26	17	1	6	18	14
	3	138	301	7	28	34	0	20	25	4	3	17	16	4
18	0	46	300	125	19	1	34	22	1	11	21	10	0	7
	1	7	210	285	1	3	50	3	4	24	13	0	6	15
19	1	0	70	348	92	9	20	18	20	10	2	14	16	4
	1	6	4	245	274	2	4	57	6	0	17	15	5	1
20	0	5	5	71	364	87	0	50	12	10	21	0	5	16
	0	2	23	0	224	267	10	31	70	2	7	13	10	12
21	0	0	13	26	41	337	96	6	90	14	1	32	0	1
	0	1	2	52	19	139	232	24	73	95	0	26	15	3
22	0	1	0	19	76	4	248	96	25	136	26	2	48	0
	0	0	4	0	70	90	35	145	24	102	127	9	58	28
23	0	0	2	6	10	135	16	115	63	32	168	48	17	78
	0	0	0	10	15	40	176	2	40	4	75	129	23	95
24	0	0	0	2	25	0	136	94	15	12	11	143	59	37
	0	0	1	2	7	63	0	156	47	0	13	13	70	16
25	0	0	0	3	0	40	42	50	142	5	5	5	58	33
	0	0	0	0	13	1	82	57	38	47	9	71	10	6
26	0	0	0	0	5	14	16	122	1	73	14	31	62	1
	0	0	0	1	1	16	41	18	127	4	3	0	59	48
27	0	0	0	0	3	1	46	6	98	60	3	0	11	89
	0	0	0	0	1	15	0	84	21	51	24	8	42	1
28	0	0	0	0	0	8	9	31	83	7	62	6	27	12
	0	0	0	0	2	2	19	38	21	91	1	0	0	60
29	0	0	0	0	1	4	2	48	1	94	28	4	0	22
	0	0	0	0	1	1	20	0	78	20	32	11	11	36
30	0	0	0	0	1	0	10	12	31	71	7	38	4	28
	0	0	0	0	0	3	6	16	50	9	67	2	1	0

[a] First entry is for J'=J''=0. Second entry is for J'=J''=100.

The band-profile calculations indicated that the difference in spin-splitting constants ($\alpha'-\alpha''$) was $\sim$0.8 in absolute value. In an attempt to explain this value, we have calculated an estimate for the X-state, using the treatment of $\Omega = 1/2$ states by Kopp and Hougen (*21*) in the manner described in previous work on XeF(*16*). We assume that the splitting in the X state is attributable to interaction with the experimentally unknown $A(^2\Pi)$ state. This state and X are the only states arising from ground term atoms, $Hg(^1S) + I(^2P)$. Theoretical calculations for the lighter HgX molecules indicate that the A state is essentially unbound (*22*). We assume that the fine structure interval in the A state is independent of internuclear distance, hence equal to the 7600 cm^{-1} for the I atom; and we assume "pure precession" which means that the constant C in Eqs. (6)–(8) of (*16*) is $\sqrt{2}$. For assumed separations of the $A(^2\Pi_{1/2})$ and X states of 7000–8000 cm^{-1}, the case c splitting constant δ for the X state ranges from 1.9 to 2.0. This constant changes very little when the separation

of the $A(1/2)$ and $A(3/2)$ states is reduced to 5000 cm^{-1}. The case c δ may be converted to an equivalent case b by using the relation $\delta = 1 - \alpha$; the resulting value is surprisingly close in absolute value to our experimental estimate. Of course we do not know what contribution to the latter is made by the B state; and we have at present no reliable way to estimate α for the B state. We hope to gain a better understanding of the effects of spin-splitting in the HgX $B \rightarrow X$ transitions from detailed rotational analyses of these systems in HgCl and HgBr, currently underway in our laboratory. In the meantime, it is clear that spin-splitting is significant, and that a basic four-branch rotational formula will be needed to account for the rotational structure.

For want of $B \rightarrow X$ data for $v'' < 5$, the X state remains poorly defined in the low-v region. To remedy this deficiency we are currently reanalyzing the $C \rightarrow X$ and $D \rightarrow X$ systems of $^{200}Hg^{127}I$, both of which sample the low-v region of the X state. We also hope to obtain improved estimates of $\mathcal{D}_e$ for the X state through direct least-squares fitting to near-dissociation expansions (*23*, *24*).

ACKNOWLEDGMENT

This work was supported by the Office of Naval Research.

RECEIVED: October 29, 1982

REFERENCES

1. J. H. PARKS, *Appl. Phys. Lett.* **31**, 297–300 (1977).
2. E. J. SCHIMITSCHEK, J. E. CELTO, AND J. A. TRIAS, *Appl Phys. Lett.* **31**, 608–610 (1977).
3. E. J. SCHIMITSCHEK AND J. E. CELTO, *Opt Lett.* **2**, 64–66 (1978).
4. K. WIELAND, *Helv. Phys. Acta.* **2**, 46–94 (1929).
5. K. WIELAND, *Helv. Phys. Acta* **14**, 420–464 (1941).
6. K. WIELAND, *Z. Elektrochem.* **64**, 761–769 (1960).
7. A. SUR AND J. TELLINGHUISEN, *J Mol. Spectrosc.* **88**, 323–346 (1981).
8. K. S. VISWANATHAN, A. SUR, AND J. TELLINGHUISEN, *J. Mol. Spectrosc.* **86**, 393–405 (1981).
9. A. SUR, A. K. HUI, AND J. TELLINGHUISEN, *J. Mol. Spectrosc.* **74**, 465–479 (1979).
10. J. TELLINGHUISEN AND J. G. ASHMORE, *Appl. Phys. Lett* **40**, 867–869 (1982).
11. J. TELLINGHUISEN, P. C. TELLINGHUISEN, S. A. DAVIES, P. BERWANGER, AND K. S. V NATHAN, *Appl. Phys Lett.*, in press.
12. M. R. MCKEEVER, A. SUR, A. K. HUI, AND J. TELLINGHUISEN, *Rev. Sci. Instrum.* **50**, 1136–1140 (1979).
13. P. BERWANGER, K. S. VISWANATHAN, AND J. TELLINGHUISEN, *J. Mol. Spectrosc.* **91**, 275–285 (1982).
14. J. TELLINGHUISEN AND S. D. HENDERSON, *Chem. Phys Lett.*, in press.
15. N.-H. CHEUNG AND T. A. COOL, *J Quant. Spectrosc. Radiat Transfer* **21**, 397–432 (1979).
16. J. TELLINGHUISEN, P. C. TELLINGHUISEN, G. C. TISONE, J. M. HOFFMAN, AND A. K. HAYS, *J. Chem. Phys.* **68**, 5177–5186 (1978).
17. G. HERZBERG, "Spectra of Diatomic Molecules," pp. 222, Van Nostrand, Princeton, N. J., 1950.
18. B. E. WILCOMB AND R. B. BERNSTEIN, *J. Mol. Spectrosc* **62**, 442–448 (1976).
19. J. TELLINGHUISEN, J. M. HOFFMAN, G. C. TISONE, AND A. K. HAYS, *J. Chem. Phys.* **64**, 2484–2490 (1976).
20. J. TELLINGHUISEN AND D. L. ALBRITTON, J. Mol. Spectrosc., **57**, 160–163 (1975).
21. I. KOPP AND J. T. HOUGEN, *Canad. J. Phys.* **45**, 2581–2596 (1967).
22. W. R. WADT, *Appl Phys Lett.* **34**, 658–660 (1979).
23. R. J. LE ROY, AND W.-H. LAM, *Chem. Phys. Lett.* **71**, 544–548 (1980).
24. J. TELLINGHUISEN, *J. Chem. Phys.*, submitted for publication.

Appendix 6

Mixed Representations for Diatomic Spectroscopic Data: Application to HgBr

by

Joel Tellinghuisen and J. Gail Ashmore
Department of Chemistry
Vanderbilt University
Nashville, Tennessee 37235

Abstract

Vibrational data for the B→X and D→X transitions of HgBr are fitted directly to expressions in which the X state is represented as a polynomial in (v+1/2) for low v and a near-dissociation expansion for high v, with smoothness constraints at crossover.

1. Introduction

It has long been standard procedure to represent the vibrational energies, rotational, and centrifugal distortion constants of diatomic molecules as polynomials in (v+1/2). The theoretical underpinning of this scheme is the Dunham treatment of the rotating oscillator [1], which is based on an expansion of the potential energy curve about its minimum. In recent years there has been increasing interest in alternative representations, with particular emphasis on schemes in which the reference energy is the dissociation limit, with the potential energy constrained to approach this limit in a theoretically sound manner [2-8]. Recent test calculations [7,8] indicate that the latter near-dissociation expansions (NDEs) are comparable to the standard polynomials in overall fit quality and efficiency, with clearly superior extrapolating ability at high v.

One minor disadvantage of the NDEs is that they do not yield directly the customary "equilibrium" constants -- ω_e, $\omega_e x_e$, B_e, α_e, etc. -- which carry physical significance and are easier to use in calculations involving only low v levels. However, these constants can be extracted algebraically from the NDEs, as has been done recently by King, *et al.* [9] in a treatment of ion-pair states. In the present paper we examine the reliability of equilibrium constants obtained in this way. We also explore another approach: the use of a mixed representation -- polynomials for low v, NDEs for high -- with incorporation of smoothness constraints at the switchover point. The calculations are performed on bandhead data for the B-X and D-X systems of HgBr, a molecule of considerable current interest as the lasant of a high-power blue-green laser [10-12]. The results obtained by fitting to the mixed representation are compared with those from the single representation (polynomial or NDE) fits, leading to the conclusion that all three representations yield essentially equivalent fit quality and equilibrium vibrational constants. The derived constants for HgBr are considered a significant improvement over previously reported parameters [13].

2. HgBr Spectra

Emission spectra were photographed for $^{200}Hg^{79}Br$ and $^{200}Hg^{81}Br$, using Tesla discharge sources and procedures described previously [13,14]. Our main concern has been the $B(^2\Sigma^+) \rightarrow X(^2\Sigma^+)$ system, which is the lasant in the HgBr laser. However, because the B state is shifted considerably to large R from the X state (see Fig. 1), the B-X emission from low v' levels does not access low v'' levels of the X state. Therefore, to achieve a more complete characterization of the X state we have photographed and reanalyzed the $D(^2\Pi_{3/2}) \rightarrow X$ system, which occurs in the 2480-2700 Å region, with strong, violet-degraded bands terminating on low v'' levels (see Fig. 1). Our analysis of the D-X system agrees with the existing interpretation [15]. However our single-isotope sources and high resolution and dispersion lead to improved precision in our measurements as compared with those of earlier workers.

To date our assignments for the B-X system include 101 bands spanning v' levels 0-13 and v'' levels 6-34. For D-X we cover v' = 0-14 and v'' = 0-16, with 72 assigned bands. Thus the two systems together span v'' levels 0-34.

3. Computations

3.1 Least-Squares Fits

The assigned bands of both systems were fitted simultaneously to expressions for the energy levels (in cm^{-1}) of all three states:

$$\nu_{BX} = E_B(v_B') - E_X(v'') \quad ; \quad \nu_{DX} = E_D(v_D') - E_X(v'') \ . \tag{1}$$

The spectra sample only the low-v regions of the B and D states, so we represented the levels of these states by the usual polynomials, e.g.,

$$E_B(v) = T_{eB} + \sum_{i=1}^{m} C_{vi}[\rho(v+1/2)]^i . \tag{2}$$

where $\rho \equiv 1.00$ for $^{200}Hg^{79}Br$ and 0.9911 for $^{200}Hg^{81}Br$. For the levels covered by our analysis, m = 2 sufficed for both the B state and the D state.

Our data sample more than 85% of the ground-state well depth, so near-dissociation expansions,

$$E_X(v) = D_{eX} - X_n(v_D-v)^{2n/(n-2)}F(v_D-v), \tag{3}$$

are appropriate representations for the X-state energy levels. In Eq. (3) X_n is a constant which depends on the coefficient C_n of the lead R^{-n} term in the long-range potential, and on the molecular reduced mass [5-7]; v_D is the (noninteger) vibrational quantum number at dissociation; and $F(v_D-v)$ is an empirical correction function, designed to go to 1.00 as $v \rightarrow v_D$. For HgBr(X) n = 6, and C_n is estimated to be 1×10^6 cm^{-1} $Å^6$ [16]. Note that the reference of energy for Eq. (3) is the X-state dissociation limit, so the constants T_{eB} and T_{eD} of the polynomial fit are replaced by T_B and T_D, the respective energies relative to this limit, in the NDE fits [7].

A number of forms have been suggested for $F(v_D-v)$ [2-8]. In the present work we have used polynomials and exponential polynomials,

$$F_a(v_D-v) = 1 + \sum_{i=1}^{m} a_i(v_D-v)^{i+q}, \tag{4a}$$

and

$$F_b(v_D-v) = \exp[\sum_{i=1}^{m} b_i(v_D-v)^{i+q}]. \tag{4b}$$

The polynomial form F_a is particularly convenient for conversion to a polynomial in (v+1/2) (see below). It is also easy to obtain good initial estimates of the adjustable parameters using this form, by fixing v_D, in which case the otherwise nonlinear fits become linear [7].

In addition to the NDE representation for the ground state, we fitted to two other representations: (1) the simple polynomial in (v+1/2), with m as large as 7; and (2) a mixed representation -- polynomial for $v'' \leq v_a''$, NDE for $v'' > v_a''$, with smoothness constraints at v_a''. The mechanics of constructing and solving the equations for the polynomial and NDE fits have been described adequately elsewhere [7,17]. However, the use of a constrained

fit in the case of the mixed representation for the X state is a slightly unconventional procedure which warrants a brief description here.

In the absence of constraints the nonlinear least-squares equations take the form,

$$\underline{d} = \underline{A}^{-1}\,\underline{Y}\ . \tag{5}$$

where the vector $\underline{d}$ contains the corrections to the current estimates of the parameters $\underline{c}_0$ (i.e., $\underline{c} \approx \underline{c}_0 - \underline{d}$), and the matrix $\underline{A}$ and vector $\underline{Y}$ are constructed as described elsewhere [7,18]. The equations are solved iteratively until $\underline{d} \approx 0$. To incorcorate the constraints we employ Lagrange's method of undetermined multipliers. In the present case we use two constraints, namely that the energies of levels v_a'' and $v_a''+1$ be the same (relative to the B-state minimum) for both X-state representations. In essence these constraints insure that $E_X(v)$ and its first derivative are continuous, which is a reasonable requirement for a vibrational energy formula. The two constraints are represented by two Lagrangian multipliers, α and β; and Eq. (5) becomes

$$\underline{d} = \underline{A}^{-1}\underline{Y} + \alpha\underline{A}^{-1}\underline{f} + \beta\underline{A}^{-1}\underline{g}\ . \tag{6}$$

where $\underline{f}^T = (\partial F/\partial d_1\ \partial F/\partial d_2\ \ .\ \ .\ \ .\ \ \partial F/\partial d_p)_0$, and similarly for $\underline{g}^T$. To calculate the adjustments to the parameters from Eq. (6) we must first determine α and β, which we do by solving the constraint equations, expressed in the form,

$$F(\underline{c}) = 0\ \ ;\ \ G(\underline{c}) = 0. \tag{7}$$

We assume that the current estimates of the parameters are close enough to the solution to permit use of the linear approximation,

$$F(\underline{c}) \simeq F(\underline{c}_0) + \underline{f}^T\underline{d}. \tag{8}$$

and similarly for $G(\underline{c})$. Substitution of $\underline{d}$ from (6) into (8) and its counterpart for $G(\underline{c})$ leads to the equations,

$$F(\underline{c}_0) - \underline{f}^T\underline{A}^{-1}\underline{Y} = \alpha\underline{f}^T\underline{A}^{-1}\underline{f} + \beta\underline{f}^T\underline{A}^{-1}\underline{g} \tag{9a}$$

$$G(\underline{c}_0) - \underline{g}^T\underline{A}^{-1}\underline{Y} = \alpha\underline{g}^T\underline{A}^{-1}\underline{f} + \beta\underline{g}^T\underline{A}^{-1}\underline{g}. \tag{9b}$$

in which the only unknowns are α and β. Solution of (9) permits calculation of $\underline{d}$ in (6), and the process is iterated until convergence is obtained.

3.2 Equilibrium Constants from NDEs

When n is even, as it is in the present case, use of (4a) for $F(v_D-v)$ permits the NDE to be recast as a finite polynomial in v, or equivalently, in (v+1/2). The resulting expressions for ω_e and $\omega_e x_e$ are

$$\omega_e = X_6 u^2\ [3 + \sum_{i=1}^{n} \binom{3+q+i}{1}\ a_i u^{i+q}] \tag{10}$$

$$\omega_e x_e = X_6 u\ [3 + \sum_{i=1}^{n} \binom{3+q+i}{2}\ a_i u^{i+q}]. \tag{11}$$

where $u = (v_D+1/2)$. For odd n and other forms of $F(v_D-v)$, equivalent expressions can be obtained from Taylor series expansions about $v = -1/2$. For example use of Eq. (4b) (F_b) leads to

$$\omega_e = X_6 u^2 F_0\ [3 + u\ f'(u)]. \tag{12}$$

and

$$\omega_e x_e = X_6 u F_0\ \{3 + 3uf'(u) + [uf'(u)]^2/2 + u^2 f''(u)/2\}. \tag{13}$$

where

$$f(u) \equiv \sum_{i=1}^{n} b_i u^{i+q}\ , \tag{14}$$

and F_0 is the value of F_b at $v = -1/2$.

4. Results and Discussion

4.1 Fit Quality and Efficiency

Preliminary fits of the D-X and B-X data separately gave nearly identical estimated variances, so in the combined fits the bands from both systems were weighted equally. As a first step in the combined fitting, we fitted to single representations (polynomial or NDE) for the X state, varying the fit order and the range of v'' covered. The variances from some of these fits are displayed in Fig. 2. In the NDE fits, exponentials (F_b) gave slightly lower variances

than did the polynomials (F_a, Fig. 2). When lead powers were dropped from the correction functions (i.e., q>0), the variance increased progressively with increasing q, for both F_a and F_b. For example, in the all-data fits to a 4-parameter F_b, the variance roughly doubled and tripled as q was increased from 0→1→2. Similar behavior occurred when selected powers were omitted within the correction function, e.g., $F_{a,4}(2,4,6,8)$ was worse than $F_{a,4}(2,4,5,6)$, which in turn was worse than $F_{a,4}(2,3,4,5)$. Thus, from the standpoint of efficiency the present data for HgBr preferred the simplest forms (q=0) of F_a and F_b.

In the polynomial fits three vibrational parameters were sufficient to v''~20. For higher v'' four parameters were needed, and additional terms produced only slight further reductions in σ^2. In the NDE fits three parameters in F sufficed down to v''~20. However four were needed for smaller v'', and five produced further significant improvement below v''~10. If we somewhat arbitrarily adopt σ^2 = 0.13 as a "minimum acceptable variance," then the 4-term polynomial representation is the most efficient, and two additional parameters (or 12 total, including v_D) are required to meet this standard using NDEs.

Initially the mixed representation fits were done with a 3-parameter polynomial in (v+1/2) and a 4-parameter NDE correction function, with switchover near v''=15. Without the constraints the variances were comparable to those of the best single representation fits; when the constraints were imposed, there was negligible increase in variance. Of course these mixed fits have more adjustable parameters than do the single representation fits, so they are less efficient. However, they have some advantages which are worth the price of the additional parameters, as discussed below.

4.2 Equilibrium Constants

As found in previous work [7] the ω_e and $\omega_e x_e$ values for the excited states were insensitive to changes in the X-state representation. In fact we used this result to advantage in obtaining initial values of the parameters in some of the nonlinear fits. It was much easier to obtain convergence in the latter when the four upper state constants and v_D were taken as known. Then by varying v_D we could obtain near-final values of the remaining parameters (two T values and the $\{a_i\}$ or $\{b_i\}$) for insertion into the full fit.

The ω_e'' and $\omega_e x_e$'' values derived from several of the fits are displayed in Fig. 3. The estimates from the NDE fits show more scatter than the polynomial results (particularly for $\omega_e x_e$) but are still in general agreement. Note that the NDE results show the same correlation that is inherent in the polynomial values, namely that high $\omega_e x_e$ values go with high ω_e values, and low with low. It is also worth noting that *none* of these sets of constants is really satisfactory for representing the levels beyond v~6, because higher-order terms become significant at this point in every case.

Weighted averages of the values in Fig. 3 yield the following "best" estimates: ω_e = 188.70(25) cm^{-1}, $\omega_e x_e$ = 1.042(12) cm^{-1}.

4.3 Dissociation Energy

The highest assigned level for HgBr(X) is still ~650 cm^{-1} or about 12% of the well depth below dissociation. In previous calculations on data sets of similar range [7], correction functions containing low-order terms in (v_D-v) failed to give satisfactory approach to dissociation, because they "turned on" too close to v_D. Here we define "satisfactory" behavior as qualitative agreement with the graphical procedure which served as a progenitor of the direct fitting methods [16,19]. The graphical method consists of extrapolating the highest observed levels to dissociation using

$$(dE_v/dv)^{2n/(n+2)} = K_n^{2n/(n+2)}(D_e-E_v), \qquad (15)$$

where $K_n = [2n/(n-2)]\ X_n^{(n-2)/2n}$. In the present case the absolute slope of the plot suggested by (15) is much higher than the theoretical limiting slope, for the highest observed levels. Accordingly all of the all-data NDE fits (including those having q = 1 or 2) yield plots of (15) which are too steep in the high-v region, as shown in Fig. 4. This is true even though Eq. (3) contains the "correct" limiting behavior, and it implies that further constraints are needed to control the approach of the correction function to dissociation.

In an attempt to achieve suitable behavior in the plots of (15), we experimented with NDE fits of only the highest observed levels. We concluded that for v''>25 a 2-parameter correction function was statistically adequate, and that q≥2 was necessary to achieve satisfactory approach to dissociation. From several fits of this type, we estimate that D_e for the X state of HgBr is 5525±75 cm^{-1}. This value is about 600 cm^{-1} below the estimate given by Wilcomb and Bernstein [16]. As was noted previously [13], the difference stems mainly from our reassignment of B-X bands terminating on high v'' levels.

4.4 Recommended Vibrational Parameters

On the basis of results discussed in the preceding paragraph, we conclude that our data for the ground state of HgBr can best be represented by a polynomial in (v+1/2) for v≤25 and an NDE having a 2-term (n=2) correction function of type (4a) for v>25. This mixed representation combines the best features of both component representations, namely the simplicity and efficiency of the polynomial for low v and the physically reasonable approach to dissociation of the NDE at high v. In the latter context it is worth reemphasizing that the all-data NDE fits did not match this performance. For example the exponential correction function containing powers 3,4,5,6,7 gave a

D_e value 55 cm^{-1} below our best estimate (see Fig. 4) and a variance 35% greater than the absolute minimum.

In Table 1 we give the results of such a mixed fit employing a 4-term polynomial for v'' = 0-25. Although the variance of this fit was a few percent higher than for a similar fit employing a 5-term polynomial, we consider the increase insignificant compared with the benefits, namely that the 4-term fit is one parameter more compact and yields ω_e, $\omega_e x_e$, and D_e values closer to our best estimates. In the v'' range covered by our data, this fit yields a 1-σ error band on $E_{v,X}$ of 0.10-0.26 cm^{-1}. The spread in values calculated from different fits, however, is somewhat larger than this, so we consider that our determination of the ground-state vibrational energy function is reliable within about 0.4 cm^{-1}.

5. Conclusion

The present calculations on vibrational data for the B-X and D-X systems of HgBr have shown that polynomials in (v+1/2), near-dissociation expansions, and mixed representations can all represent the ground-state energy levels with equivalent fit quality. The mixed representations are two parameters less compact than the NDEs, which in turn are two parameters less compact than the polynomials. However, in spite of their relative inefficiency, the mixed representations have advantages which justify the additional parameters. There may well be other applications in which the mixed representation can rival the single representations in compactness. The fits to the mixed representation involve the use of nonlinear least squares with constraints, for which the equations can be set up straightforwardly using procedures we have outlined.

The spectroscopic constants given in Table 1 are considered reliable within ~0.4 cm^{-1} for the calculation of bandheads in the B-X and D-X systems of $^{200}Hg^{79}Br$, for the stated ranges of v. These parameters should be equally

reliable for other isotopomers of HgBr. through use of the standard isotopic relations [13,17]. We are currently trying to extend the B-X assignments to higher v'', in order to better determine the ground-state dissociation energy. We hope to publish the full analysis in the near future.

Acknowledgment

This work was supported by the Office of Naval Research.

References

[1] J. L. Dunham, Phys. Rev. 41 (1932) 721.

[2] A.-R. Hashemi-Attar, C. L. Beckel, W. N. Keepin, and S. A. Sonnleiter, J. Chem. Phys. 70 (1979) 3881.

[3] A.-R. Hashemi-Attar and C. L. Beckel, J. Chem. Phys. 71 (1979) 4596.

[4] C. L. Beckel and R. B. Kwong, J. Chem. Phys. 73 (1980) 4698.

[5] R. J. Le Roy and W.-H. Lam, Chem. Phys. Lett. 71 (1980) 544.

[6] J. W. Tromp and R. J. Le Roy, Can. J. Phys. 60 (1982) 26.

[7] J. Tellinghuisen, J. Chem. Phys. 78 (1983) 2374.

[8] J. W. Tromp and R. J. Le Roy, to be published.

[9] G. W. King, N. T. Littlewood, and I. M. Littlewood, Chem. Phys. (in press).

[10] J. H. Parks, Appl. Phys. Lett. 31 (1977) 297.

[11] E. J. Schimitschek, J. E. Celto, and J. A. Trias, Appl. Phys. Lett. 31 (1977) 608.

[12] E. J. Schimitschek and J. E. Celto, Opt. Lett. 2 (1978) 64.

[13] J. Tellinghuisen and J. G. Ashmore, Appl. Phys. Lett. 40 (1982) 867.

[14] J. Tellinghuisen, Paper MB9, Topical Meeting on Excimer Lasers (1983), (to be published).

[15] K. P. Huber and G. Herzberg, *Constants of Diatomic Molecules*, Van Nostrand Reinhold, New York (1979).

[16] B. E. Wilcomb and R. B. Bernstein, J. Mol. Spectrosc. 62 (1976) 442.

[17] K. S. Viswanathan and J. Tellinghuisen, *J. Mol. Spectrosc. (in press)*.

[18] W. E. Deming, *Statistical Adjustment of Data*, Dover Publications, New York (1964).

[19] J. Tellinghuisen, J. M. Hoffman, G. C. Tisone, and A. K. Hays, J. Chem. Phys. 64 (1976) 2484.

Table 1. Recommended vibrational parameters (cm^{-1}) for X, B, and D states of $^{200}Hg^{79}Br$.[a,b]

	X($^2\Sigma^+$)	B($^2\Sigma^+$)	D($^2\Pi_{3/2}$)
T_e	0	23488.98(23)	38572.81(19)
T		17961.82(17.71)	
D_e	5527.16(17.72)		
ω_e	188.915(90)	135.953(44)	231.230(44)
$\omega_e x_e$ ($-c_{v2}$)	1.0589(146)	0.2544(33)	0.9898(33)
c_{v3}	-1.9302×10^{-3}		
c_{v4}	-2.2678×10^{-4}		
v_D	65.031(486)		
X_6	0.0186		
a_1	1.6605×10^{-5}		
a_2	-3.0609×10^{-7}		
σ		0.36	
v range	0-34	0-13	0-14
no. of bands	173	101	72

[a]Results from fit to mixed representation for X state- polynomial for $v \leq 25$, NDE (Eq. 4a, q=2) for $v > 25$. Where given, the figures in parentheses represent the 1-σ errors in terms of last figures. Parameters are given to sufficent precision to reproduce calculated band heads within 0.1 cm^{-1}.

[b]Raw data available on request.

Figure Captions

Figure 1: Potential diagram for HgBr, showing levels of the X, B, and D states spanned by the present analysis. Note the different energy scales for all three states.

Figure 2: Variance of single representation fits as a function of v'' range covered. The indicated v'' represents the maximum included in the polynomial fit, the minimum included in the NDE fit. For clarity the polynomial results have been shifted up (scale to right).

Figure 3: ω_e'' and $\omega_e x_e$'' values from various single representation all-data fits. Error bars represent 1 σ.

Figure 4: Plot suggested by Eq. (15) for final recommended X-state parameters (points and solid curve), and for two all-data NDE fits: $F_{a,5}(q=0)$ (dashed curve) and $F_{b,5}(q=2)$ (dotted curve). Also shown is the theoretical limiting line (T).

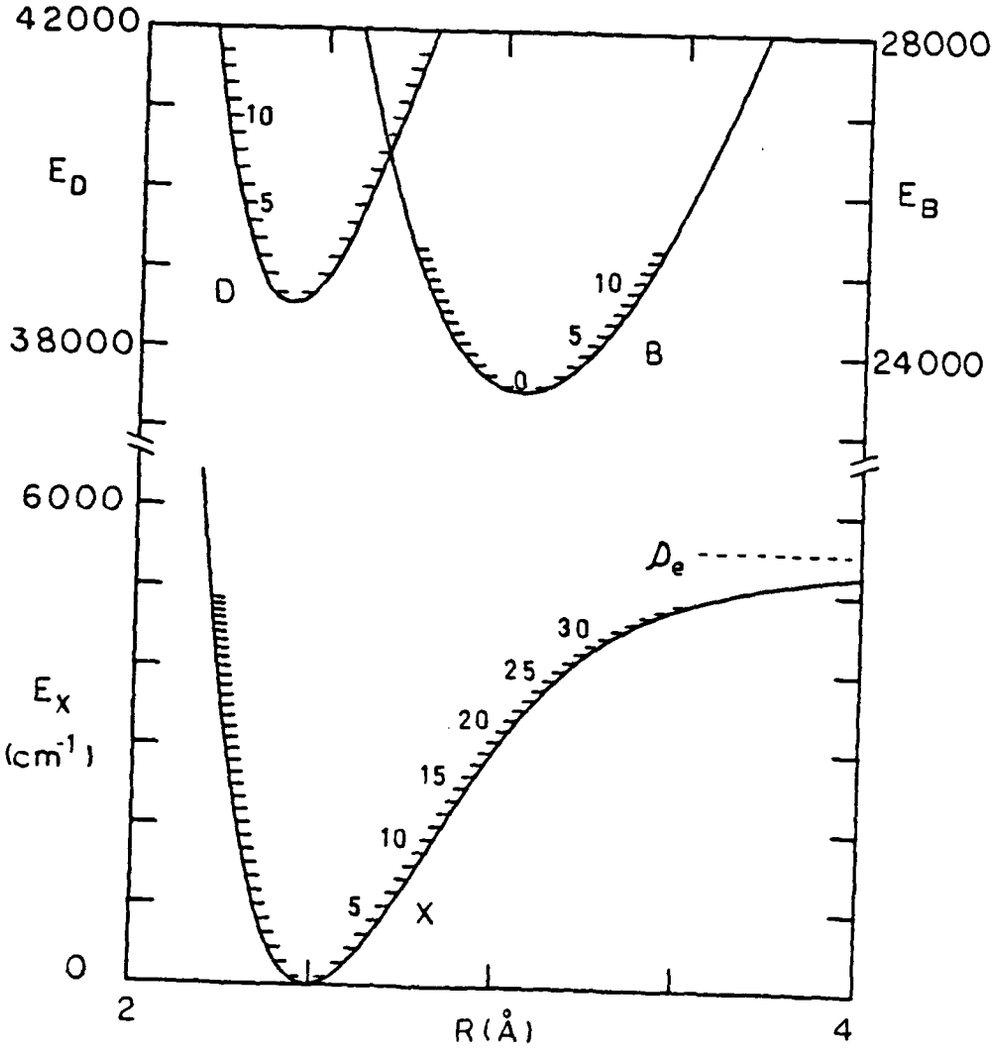
42000
38000
6000
0
28000
24000
E_D
E_B
E_X
(cm^{-1})
D
B
X
D_e
10
5
0
30
25
20
15
2
4
R(Å)

Fig 1

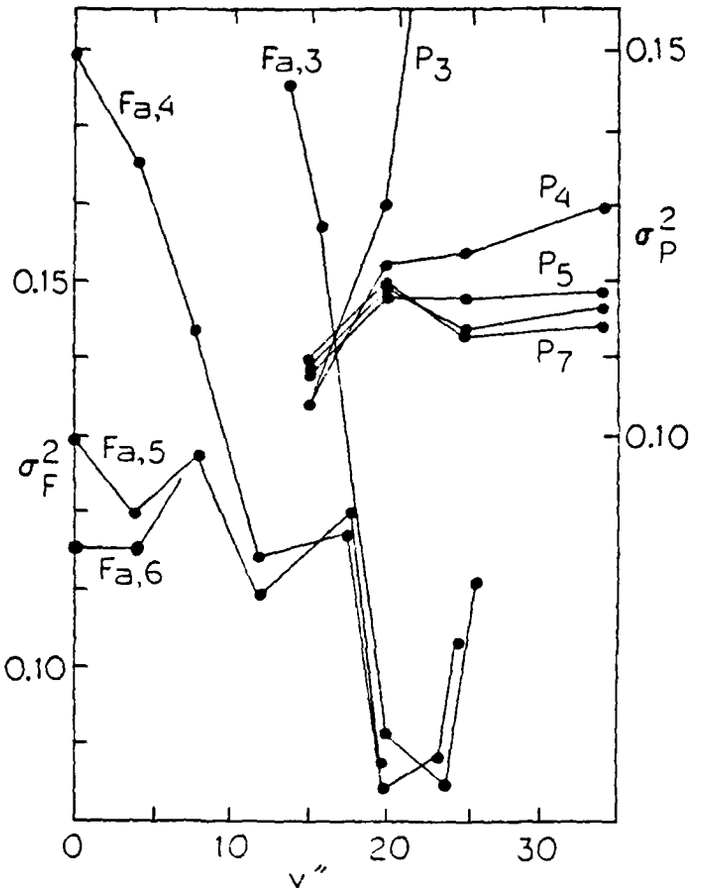
Fa,3
P_3
Fa,4
P_4
P_5
P_7
Fa,5
Fa,6
σ_F^2
σ_P^2
0.15
0.10
0
10
20
30
v''

Fig. 2

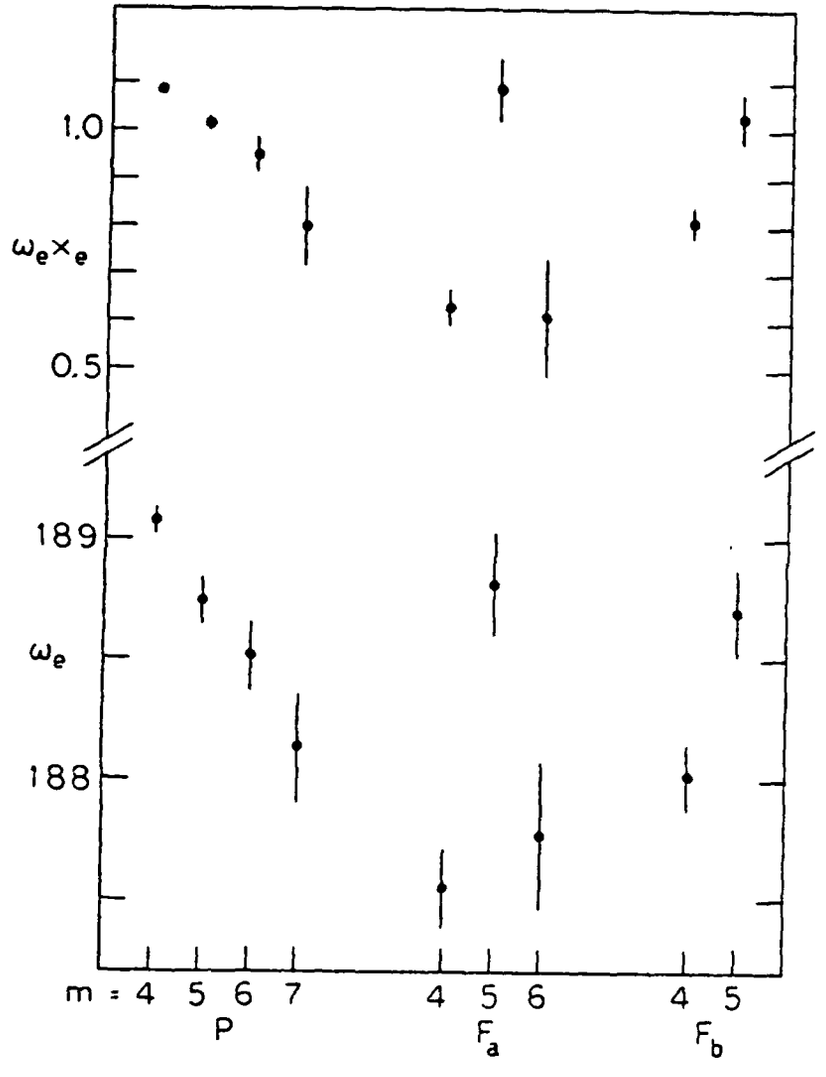
1.0
$\omega_e x_e$
0.5
189
ω_e
188
m = 4 5 6 7 4 5 6 4 5
P
F_a
F_b

Fig 3

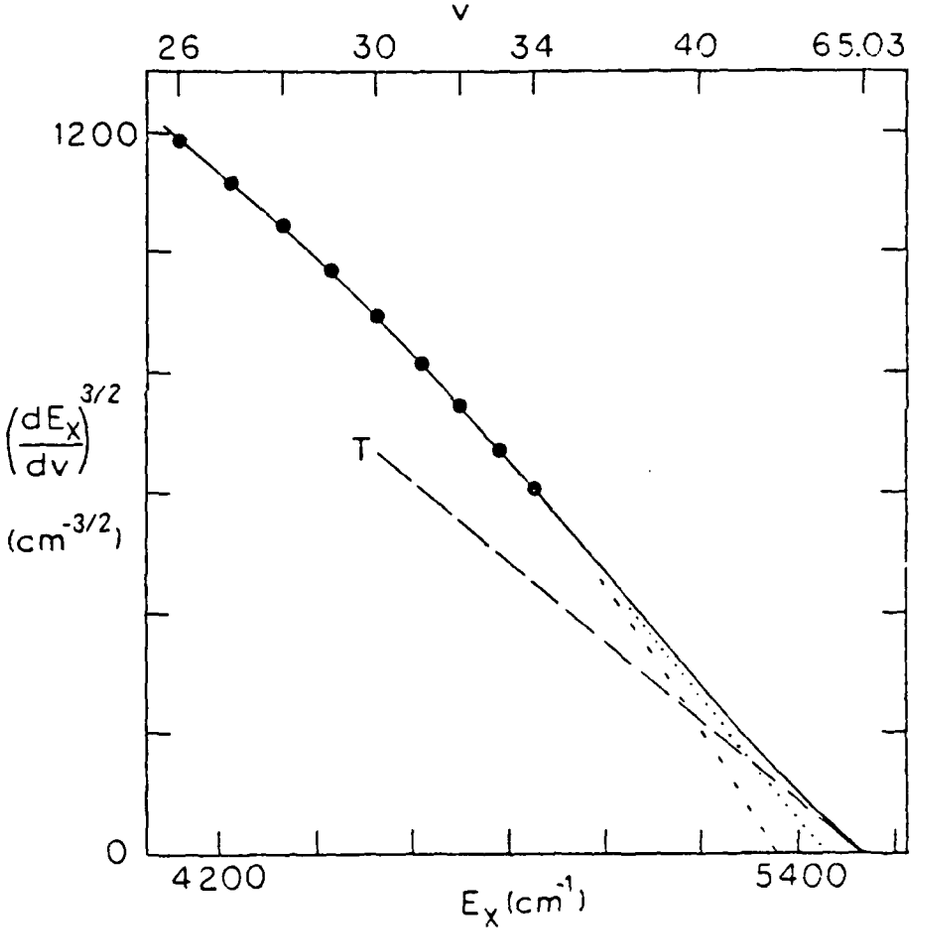
v
26
30
34
40
65.03
1200
$\left(\frac{dE_X}{dv}\right)^{3/2}$
$(cm^{-3/2})$
T
0
4200
5400
$E_X (cm^{-1})$

Fig. 4

Appendix 7

FB1. (8:30)

"BEST" SPECTROSCOPIC CONSTANTS FOR HgBr FROM DIRECT FITS OF MULTIPLE BAND SYSTEMS TO POLYNOMIALS AND NEAR-DISSOCIATION EXPANSIONS*

J. GAIL ASHMORE AND JOEL TELLINGHUISEN

The B→X (4200-5100 Å), C→X (2700-2950 Å), and D→X (2480-2700 Å) transitions of HgBr have been photographed and analyzed for isotopically pure $^{200}Hg^{79}Br$ and $^{200}Hg^{81}Br$. The analyses yield improved vibrational constants for all four states and rotational constants for the B and X states. Optimal spectroscopic parameters are obtained for all four states from direct, simultaneous fits of all three transitions to the standard polynomials in (v+1/2) and to near-dissociation expansions.[1,2]

In addition to the above-mentioned systems, we have recorded and analyzed by computer simulation the B→A transition (5500-8000 Å). Efforts are currently underway to (1) measure collisional line broadening in the B→X system using a Fabry-Perot interferometer, and (2) determine the R-dependence of the B→X transition strength function from analysis of relative intensity data.

---

* Work supported by the Office of Naval Research.
[1] R. J. Le Roy and W-H. Lam, Chem. Phys. Lett. 71, 544 (1980).
[2] J. Tellinghuisen, J. Chem. Phys. (in press).

Address of Authors: Department of Chemistry, Vanderbilt University, Nashville, TN 37235.

FB2. (8:47)

INTERFACING A MICRODENSITOMETER TO A MICROCOMPUTER*

C. CARLYSLE SALTER AND JOEL TELLINGHUISEN

In methods of photographic spectroscopy there is a need for precision measurement of a large amount of experimental data -- the positions and intensities of rotational lines, vibrational band heads, and calibration lines on the photographic plate. Microdensitometers and optical comparators permit one to measure the positions of sharp features with a precision of 1-2 μm; however, the procedure of measuring, recording, and logging the data for further computer processing can be very tedious and time consuming, if done manually. To expedite this aspect of our work, we have designed and built a cheap (~$2500, microcomputer included) control interface, by means of which a TRS-80 Model III microcomputer controls the motion of the plate on a microdensitometer and logs the optical density in digital form. In this paper we discuss various aspects of the interfacing task, including hardware and software for stepping motor control, analog-to-digital conversion, and extraction of line positions from the recorded data.

---

* Work supported by the Office of Naval Research.

Address of Authors: Department of Chemistry, Vanderbilt University, Nashville, TN 37235.

END

FILMED

9-83

DTIC